Cytotoxic CD4$^+$ T cells driven by T-cell intrinsic IL-18R/MyD88 signaling predominantly infiltrate *Trypanosoma cruzi*-infected hearts

Carlos-Henrique. D. Barbosa[1,2*], Fábio B. Canto[1,3*], Ariel Gomes[1,4*], Layza M. Brandão[1], Jéssica R. Lima[1], Guilherme A. Melo[1], Alessandra Granato[1,5], Eula G.A. Neves[6], Walderez O. Dutra[6], Ana C. Oliveira[7], Alberto Nóbrega[1] and Maria Bellio[1]**.

[1]Department of Immunology, Instituto de Microbiologia Paulo de Góes, Universidade Federal do Rio de Janeiro (UFRJ), Rio de Janeiro, RJ, 21941-902 Brazil; Ph: +55-21-987496559

[2]present address: Department of Microbiology & Immunology, Chicago Medical School, Rosalind Franklin University of Medicine and Science, Chicago, IL, USA.

[3]present address: Departamento de Imunobiologia, Instituto de Biologia, Universidade Federal Fluminense (UFF) Niterói, RJ 24210-350, Brazil.

[4]present address: Faculdade de Medicina da Universidade Estácio de Sá, Angra dos Reis, RJ Brazil.

[5]present address: The Hospital for Sick Children - Genetics and Genome Biology. Toronto, ON, Canada

[6]Laboratório de Biologia das Interações Celulares, ICB, Universidade Federal de Minas Gerais, Belo Horizonte, MG, Brazil

[7]Instituto de Biofísica Carlos Chagas Filho, UFRJ, Rio de Janeiro, RJ, Brazil.

Keywords: Infectious disease**,** cytotoxicity, myocarditis, parasite, tissue immunity.

* These authors contributed equally to this work

***Corresponding Author and Lead Contact*:

e-mail: belliom@micro.ufrj.br or mariabellioufrj@gmail.com

Abstract:

Increasing attention has been directed to cytotoxic $CD4^+$ T cells (CD4CTLs) in different pathologies, both in humans and mice. The impact of CD4CTLs in immunity and the mechanisms controlling their generation, however, remain poorly understood. Here, we show that CD4CTLs abundantly differentiate during mouse infection with the intracellular parasite *Trypanosoma cruzi*. CD4CTLs display parallel kinetics to Th1 cells in the spleen, mediate specific cytotoxicity against cells presenting pathogen-derived antigens and express immunoregulatory and/or exhaustion markers. We demonstrate that CD4CTL absolute numbers and activity are severely reduced in both *Myd88*$^{-/-}$ and *Il18ra*$^{-/-}$ mice. Of note, the infection of mixed-bone marrow chimeras revealed that WT but not *Myd88*$^{-/-}$ cells transcribe the CD4CTL gene signature and that *Il18ra*$^{-/-}$ and *Myd88*$^{-/-}$ $CD4^+$ T cells phenocopy each other. Moreover, adoptive transfer of WT $CD4^+GzB^+$ T cells to infected *Il18ra*$^{-/-}$ mice extended their survival. Importantly, cells expressing the CD4CTL phenotype predominate among $CD4^+$ T cells infiltrating the infected mouse cardiac tissue and are increased in the blood of Chagas patients, in which the frequency of CD4CTLs correlates with the severity of cardiomyopathy. Our findings describe CD4CTLs as a major player in immunity to a relevant human pathogen and disclose T-cell intrinsic IL-18R/MyD88 signaling as a key pathway controlling the magnitude of the CD4CTL response.

50 **Introduction:**

51 CD4CTLs are present in viral infections, cancer and autoimmune diseases
52 (Cheroutre & Husain, 2013; Juno et al., 2017; Takeuchi & Saito, 2017). Although more
53 frequently found in chronic conditions, CD4CTLs have also been described during
54 acute viral infection (Brien et al., 2008; Brown et al., 2012; Fang et al., 2012; Jellison,
55 et al., 2005; Wilkinson et al., 2012). At present, however, there are few studies on the
56 CD4CTL response to infection with non-viral intracellular pathogens (Burel et al.,
57 2016; Canaday et al., 2001; Kotov et al., 2018; Krueger et al., 2021). The role of
58 CD4CTLs in immunity against intracellular parasites and the mechanisms operating in
59 the generation and maintenance of this cell subset are poorly understood.

60 Following the recognition of the cognate antigen-MHC complex and under the
61 influence of cytokines secreted by antigen presenting cells (APCs), naïve $CD4^+$ T cells
62 proliferate and differentiate into diverse subsets, including Tfh, Th1, Th2 or Th17, with
63 varied effector functions. Different pathogen-derived molecular patterns (PAMPs) elicit
64 distinct innate immune pathways, resulting in tailored Th responses against the
65 infectious agent (Kara et al., 2014). Interestingly, single-cell heterogeneity in the
66 transcriptional profile of effector $CD4^+$ T cells, dictated in a microbe-specific manner,
67 has been recently found in the gut (Kiner et al., 2021). Additionally, tissue-derived
68 factors can also be involved in defining $CD4^+$ T cell phenotypes (Poholek, 2021). In this
69 context, the mechanism regulating the differentiation of CD4CTLs remains an open and
70 relevant question. Although some authors consider CD4CTLs functional variants of
71 Th1 cells, there is also evidence that CD4CTLs might constitute a Th1-independent
72 subset, directly differentiating from naïve $CD4^+$ T cell precursors, or even a
73 heterogeneous population congregating cytolytic lymphocytes that originate from

74 different T-cell subsets, such as Treg, Th1 and Th2 cells [reviewed in (Cheroutre &
75 Husain, 2013) and (Takeuchi & Saito, 2017)].

76 Receptors belonging to the TLR and IL-1R families are upstream of the MyD88
77 adaptor molecule and are expressed both in myeloid and lymphoid cell lineages.
78 MyD88-dependent signaling in innate cells can influence Th1 cell differentiation by
79 inducing the release of IL-12 or IFN-γ (Joffre et al., 2009; Takeda et al., 1998). The T-
80 cell intrinsic MyD88 adaptor function was also shown to be essential for the Th1
81 response in different contexts. The identity of the receptor acting upstream of MyD88
82 on T cells, however, was not always determined (Frazer et al., 2013; LaRosa et al.,
83 2008) and remains a matter of debate. Early *in vitro* studies have shown that IL-18
84 synergizes with IL-12 in the induction of IFN-γ production and T-bet expression by
85 $CD4^+$ T cells and, therefore, impacts Th1 development (Robinson et al., 1997).
86 Intriguingly, however, the IL-18 contribution for a robust Th1 response *in vivo* has not
87 always been confirmed (Haring & Harty, 2009; Monteforte et al., 2000). ST2 (IL-33
88 receptor) and IL-1R have also been implicated in the establishment of Th1 responses to
89 viral infection (Baumann et al., 2015) and immunization (Ben-Sasson et al., 2009;
90 Schenten et al., 2014), respectively. Previously, our group identified the crucial role of
91 T cell-intrinsic IL-18R/MyD88 signaling for the reinforcement and maintenance of the
92 Th1 program *in vivo,* in response to mouse infection with *Trypanosoma cruzi,* in which
93 Th1 cells have a key protective function (Oliveira et al., 2017; Rodrigues et al., 2012).

94 *T. cruzi* is an intracellular protozoan parasite and the etiologic agent of Chagas
95 disease (*American trypanosomiasis*), one of the most important parasitic diseases in the
96 Western Hemisphere. Chagas disease is an important cause of heart failure, stroke,
97 arrhythmia and sudden death, being the leading cause of cardiomyopathy among
98 younger individuals in Latin America (Bern, 2015; Nunes et al., 2018). Here we

99 showed that, $CD4^+$ T lymphocytes with a CTL phenotype are abundantly present in the
100 spleen of mice infected with *T. cruzi* and display *in vitro* and *in vivo* Ag-specific
101 cytotoxicity against APCs. Of note, we found that cells with a CTL phenotype
102 predominate among $CD4^+$ T lymphocytes infiltrating infected cardiac tissue. Using
103 mixed bone marrow (mix-BM) chimeras, we show that T cell-intrinsic IL-18R/MyD88
104 signaling plays a crucial role for the expansion/survival of $CD4^+$ T cells expressing the
105 CTL gene signature *in vivo*. In accordance with results obtained in mix-BM chimeras,
106 we found that absolute numbers of CD4 T cells displaying cytotoxic markers and
107 activity were severely reduced in *Myd88*$^{-/-}$ and *Il18ra*$^{-/-}$ mouse lineages. Moreover,
108 adoptive transfer of WT $CD4^+GzB^+$ T cells to *Il18ra*$^{-/-}$ mice increase survival of this
109 susceptible mouse strain to infection. Interestingly, the majority of $CD4^+GzB^+$ T cells in
110 WT infected mice express high levels of immunoregulatory molecules such as, Tim-3,
111 Lag-3, CD39 and PD-1. Finally, and importantly, we detected the presence of $CD4^+$ T
112 cells expressing perforin in the blood of patients with the severe cardiac form of Chagas
113 disease and correlation analyses point to a possible pathogenic role of these cells in the
114 chronic phase of Chagas myocarditis. To our knowledge, the present study is the first to
115 extensively characterize CD4CTLs generated in response to a protozoan pathogen in a
116 murine model and to elucidate a central mechanism that accounts for their
117 expansion/survival.
118
119 **Results:**
120 ***$CD4^+$ T cells with cytolytic phenotype are abundantly present in the spleen of mice***
121 ***infected with T. cruzi***
122 CD4CTLs express granzyme B (GzB) and perforin (PRF), which are major
123 constituents of CD8CTL and NK cell-granules that promote target cell death in a

124 number of ways (Afonina et al., 2010). Here, we reveal the presence of a
125 TCRαβ$^+$CD8α$^-$NK1.1$^-$CD4$^+$GzB$^+$ T cell population, which represents around 30% of
126 the CD4$^+$ T cells in the spleen of C57BL/6 (B6) mice, in the acute phase of infection
127 with *T. cruzi* **(Figures 1A** and **1B)**. Equivalent percentages of CD4$^+$PRF$^+$ T cells were
128 found (**Figure 1C)** and the majority of CD4$^+$GzB$^+$ T cells express PRF and the cytolytic
129 marker 2B4 (CD244) (**Figures 1D** and **1E** and Figure 1-figure supplement 1A). Of
130 note, most CD4$^+$GzB$^+$ T cells (> 80%) do not express IFN-γ at day 14 post-infection
131 (pi), the peak time-point of the T cell response, and although CD4GzB$^+$ and CD4IFN-γ$^+$
132 cells follow similar kinetics in the spleen, the absolute number of CD4$^+$GzB$^+$ T cells
133 was superior to that of CD4$^+$IFN-γ$^+$ cells, at every time point of the infection (**Figures**
134 **1F** and **1G**). It is known that intracellular parasitism by *T. cruzi* Y strain in the spleen is
135 at its highest point between day 12 and 15 pi, concomitant with the histologically
136 observed massive destruction of parasitized splenic macrophages (Cordeiro et al., 1997).
137 Therefore, there is a coincidence between parasite titers in the spleen and the frequency
138 and absolute numbers of CD4$^+$GzB$^+$ T cells. We also observed an increase in the
139 percentage of degranulating CD4$^+$ T cells at day 14 pi, comparable to the CD8$^+$ T cells,
140 as inferred by staining with anti-CD107a (LAMP-1) mAb, **(Figure 1H)**, although
141 CD8CTLs are present at higher percentage (Figure 1-figure supplements 1B-E and 1G)
142 and absolute number (Figure 1-figure supplements 1F and 1H). In summary, these data
143 show the remarkable induction of CD4$^+$ T cells with cytolytic potential during infection
144 with *T. cruzi*, an effector subpopulation whose appearance in the spleen parallels and
145 largely outnumbers that of classic GzB-negative IFN-γ$^+$ Th1 cells.

146 ***CD4$^+$ T cells from infected spleen exert Ag-specific cytotoxicity***

147 To ascertain the presence of CD4$^+$ T lymphocytes with cytolytic function, we

148 performed a redirected cytotoxicity assay, with anti-CD3 mAb–coated B cell blasts as
149 target cells that were co-incubated with either highly purified effector ($CD44^{hi}$) CD4 T
150 cells sorted from the spleen of infected mice, or naive ($CD44^{lo}$) CD4 T cells from non-
151 infected controls. The CTL activity was observed only when effector $CD4^+$ T cells were
152 employed (**Figure 2A**). In order to determine if the CD4CTL killing capability is
153 dependent on GzB- and PRF-mediated killing, we performed the cytotoxic assays in the
154 presence of the GzB and PRF inhibitors, Z-AAD-CMK and Concamycin A,
155 respectively. As shown in **Figure 2-figure supplement 1A,** the killing of target cells
156 was abolished in this condition, demonstrating that the cytolysis mediated by CD4CTLs
157 in *T. cruzi*-infected mice depends on GzB and PRF, as previously shown for tumor-
158 specific CD4CTLs (Quezada et al. 2010). Antigen-specific cytotoxicity, using highly
159 purified $CD4^+$ T cells, was also assayed *in vitro* against an I-A^{b+} macrophage cell line
160 (IC-21), loaded or not with *T. cruzi* amastigote total protein extract. Results shown in
161 **Figure 2B** and **Figure 2-figure supplement 1B** demonstrate that CD4CTLs with
162 cognate cytotoxic activity are present in the spleen of infected mice. FasL is expressed
163 on $CD8^+$ and $CD4^+$ T cells at the immunological synapse following Ag-triggered
164 degranulation and participates in CD4CTL-mediated lysis of target cells (Bossi &
165 Griffiths, 1999; Brown et al., 2009; Kotov et al., 2018). As shown in **Figure 2B,**
166 addition of anti-FasL mAb significantly inhibited the specific lysis of the target cells,
167 demonstrating the involvement of the FasL/Fas pathway in the killing process.

168 We tested the *in vivo* killing of target splenocytes loaded with class II-restricted
169 peptides (SA85-1.1c and d), derived from a protein of the *T. cruzi* transialidase
170 superfamily (Millar & Kahn, 2000) (**Figure 2C** and **Figure 2-figure supplement 1C).**
171 The detailed Ag-specific repertoire of CD4CTLs could not be further assessed because
172 of the scarce definition of parasite-derived CD4 epitopes in the literature. To

173 circumvent this, we infected mice with ovalbumin (OVA)-expressing Y strain
174 trypomastigotes (Y-OVA) (Gomes-Neto et al., 2018) and compared the *in vivo*
175 cytotoxic response against known OVA-derived CD4 and CD8 epitopes: $OVA_{323-339}$ and
176 $OVA_{257-264}$, respectively. As shown in **Figure 2D**, the same level of specific killing was
177 attained against targets loaded with class I- or class II-restricted OVA peptides.
178 Together, these experiments confirmed the presence of a $CD4^+$ T cell population with
179 Ag-specific cytolytic function against MHC class II-restricted epitopes in the spleen of
180 mice infected with *T. cruzi.*
181
182 ***$CD4^+GzB^+$ T cells express transcription factors typical of CTLs***
183 We then investigated the expression of transcription factors (TFs) typical of
184 cytotoxic CD8 T cells. T-bet and Eomesodermin (Eomes) are known to bind to the
185 promoters of *Gzmb* and *Prf1* (Glimcher et al., 2004; Intlekofer et al., 2005; Pearce et al.,
186 2003) and were shown to be expressed in CD4CTLs (Curran et al., 2013; Eshima et al.,
187 2012; Qui et al., 2011). **Figures 2E** and **2F** show that the vast majority of $CD4^+GzB^+$ T
188 cells express T-bet, but not FoxP3, the master gene of Treg cells. In accordance with the
189 cytolytic potential of $CD4^+GzB^+$ T cells in our model, 60% of the $CD4^+GzB^+$ T cells
190 express Eomes, while only a small percentage of GzB-negative $CD4^+$ T cells are
191 $Eomes^+$ (**Figure 2G**). Of note, at day 14 pi, the vast majority of both GzB^+ and GzB-
192 negative $CD4^+$ T lymphocytes are $CD44^{hi}CD62L^{lo}$ effector/memory cells (Figure 2-
193 figure supplement 2).
194 CD4CTLs that migrate to the gut, gradually stop expressing ThPOK, while
195 upregulating the expression of RUNX3 (Mucida et al., 2013; Reis et al., 2013), which is
196 known to drive the CTL gene program in $CD8^+$ T cells (Cruz-Guilloty et al., 2009;
197 Egawa et al., 2007). The long-form transcript encoding RUNX3 (*Runx3d*) is also

198 expressed in Th1 cells, but not in Th2 or naïve cells (Djuretic et al., 2007). As shown in
199 **Figure 2H**, besides *Runx3d* mRNA, we found that $CD4^+GzB^+$ T cells, sorted from the
200 spleen of tamoxifen-treated and infected GzmbCreER^{T2}/ROSA26EYFP reporter mice
201 (Bannard et al., 2009) (Figure 2-figure supplement 3A), express ThPOK *(Zbtb7b gene)*-
202 coding RNA comparable to naive $CD4^+$ T cells, at day 14 pi, when their number and
203 frequency are at the highest levels in this organ (**Figure 1G**). The absence of CD8α-
204 coding transcripts confirms the purity of sorted $CD4^+GzB^+$ T cells (Figure 2-figure
205 supplement 3B). These data show that $CD4^+GzB^+$ T cells generated in response to
206 infection with *T. cruzi,* besides expressing cytolytic markers, also express T-bet, Eomes
207 and RUNX3, typical TFs found in cytotoxic T cells.
208
209 ***$CD4^+GzB^+$ T cells express cytotoxic markers and immunoregulatory molecules***
210 Tr1 cells are a subset of IL-10-producing $CD4^+FoxP3^-$ T cells that express GzB and
211 PRF and exert a potent suppressive function both in humans and mice (Roncarolo et al.,
212 2018). Since a high percentage of $CD4^+GzB^+$ T cells in our system express Eomes,
213 which drives the development of Tr1 cells (Zhang et al., 2017), we investigated whether
214 *T. cruzi*-induced $CD4^+GzB^+$ T cells would share other phenotypic characteristics with
215 Tr1 cells. We detected a very low frequency of IL-10-producing $TCR\alpha\beta^+CD4^+$ T cells
216 in the spleens of mice infected with *T. cruzi*, in agreement with previous data (Jankovic
217 et al., 2007), although IL-10^+ cells were found to be more frequent among $CD4^+GzB^+$ T
218 cells (**Figures 3A** and Figure 3-figure supplement 1A-B). The co-expression of LAG-3
219 and CD49b defines both human and mouse Tr1 cells (Gagliani et al., 2013). Although
220 most splenic $CD4^+GzB^+$ T cells express LAG3, only a minor percentage of these cells
221 co-express CD49b (**Figures 3B** and **3C** and Figure 3-figure supplement 1C). On the
222 other hand, a substantial fraction of splenic $CD4^+GzB^+$ T cells express the

223 immunoregulatory molecule TIM-3 and downregulate CD27 (**Figures 3D** and **3E**),
224 indicating that these might be terminally differentiated cells, as suggested in other
225 models (Anderson et al., 2016; Takeuchi & Saito, 2017).

226 Natural killer group 2 (NKG2) members A, C, D and E are C-type lectin-like
227 receptors and cytotoxic markers expressed by NK, NKT, γδ and activated $CD8^+$ T cells
228 (Gunturi et al., 2004; Stojanovic et al., 2018). NKG2C/E and NKG2D molecules
229 identify a CD4CTL population, present in mouse lungs during influenza A virus (IAV)
230 infection (Marshall et al., 2017). As shown in **Figures 3F** and **3G**, the fraction of cells
231 expressing NKG2A/C/E and NKG2D was increased among splenic $CD4^+GzB^+$ T cells,
232 when compared to either GzB-negative $CD4^+$ T cells of infected mice, or to naive $CD4^+$
233 T cells of non-infected controls (Figure 3-figure supplement 2A and 2B). The class I-
234 restricted T cell associated molecule (CRTAM) was described as being critical for the
235 differentiation of CD4CTLs (Takeuchi et al., 2016; Takeuchi & Saito, 2017). **Figure**
236 **3H** shows that the frequency of CRTAM-expressing cells was also increased among
237 splenic $CD4^+GzB^+$ T cells of *T. cruzi*-infected mice, when compared with GzB-negative
238 $CD4^+$ T cells. We then analyzed whether CRTAM and NKG2X cytotoxic markers were
239 co-expressed on GzB^+CD4^+ T cells. As shown in Figure 3-figure supplement 3, while
240 most $NKG2D^+$ cells also express the CRTAM cytotoxic marker, only a minority of
241 $CD4^+GzB^+$ T cells co-express CRTAM and NKG2A/C/E molecules. The frequencies of
242 $CRTAM^+$, $NKG2A/C/E^+$ and $NKG2D^+$ $CD8^+GzB^+$ T cells in infected mice are shown
243 in Figure 3-figure supplement 4. Since, as shown in Figure 2-figure supplement 2, both
244 GzB^- and GzB^+ $CD4^+$ T cells are in their majority effector/effector memory cells at day
245 14 pi, equivalent results were obtained gating on $CD44^{hi}$ cells or not (Figure 3-figure
246 supplement 5). Together, these results show that a significant fraction of the $CD4^+GzB^+$
247 T cell subpopulation found in this unicellular parasite infection model complies with

248 the general phenotype of CD4CTLs and CD4CTL-precursors reported in response to
249 viral infection.
250
251 ***CD4CTLs are present in lower numbers in Myd88$^{-/-}$ infected mice***
252 To extend our understanding on the requirements for the differentiation of
253 CD4CTLs and their relationship to Th1 cells, we next investigated the role of IL-12,
254 IFN-γ and MyD88 in their generation. IL-12 and IFN-γ are the major cytokines driving
255 Th1 differentiation and T-bet expression, but their requirement for CD4CTL generation
256 is controversial (Brown et al., 2009; Cooper et al., 2004; Curran et al., 2013; Hua et al.,
257 2013; Kotov et al., 2018; Krueger et al., 2021; Tagawa et al., 2016; Xie et al., 2010).
258 Here, we observed that *Il12p40$^{-/-}$* mice infected with *T. cruzi* displayed lower
259 percentages of T-bet^{+}CD4^{+} and IFN-γ^{+}CD4^{+} T cells and exhibited very low levels of
260 CD4^{+}GzB^{+} T cells (**Figure 4A**). Interestingly, in infected *Ifng$^{-/-}$* mice, despite the lower
261 frequency of T-bet^{+}CD4^{+} T cells, CD4^{+}GzB^{+} T cells attained the same frequencies as
262 observed in the spleens of WT animals (**Figure 4B**). However, absolute numbers of
263 both total CD4^{+} and CD4^{+}GzB^{+} T cells were lower in *Ifng$^{-/-}$* mice when compared to
264 WT controls. Thus, both IL-12p40 and IFN-γ play important but distinct roles in the
265 differentiation and expansion/survival of CD4^{+}GzB^{+} T cells.
266 The above results obtained in *Il12p40$^{-/-}$* and *Ifng$^{-/-}$* mice, together with the fact that
267 *Myd88$^{-/-}$* mice have lower levels of Th1 cells and are highly susceptible to infection with
268 *T. cruzi* (Campos et al., 2004; Oliveira et al., 2010), prompted us to address the role of
269 MyD88-dependent pathways in the generation of CD4CTLs. Although infected *Myd88^{-}*
270 *$^{/-}$* mice displayed equivalent absolute numbers and percentages of total splenic CD4^{+} T
271 cells when compared to WT mice (Figure 4-figure supplement 1A), the frequencies and
272 absolute numbers of CD4^{+}GzB^{+} T cells were significantly lower in this mouse strain

273 (**Figures 4C-4E)**. Furthermore, absolute numbers of CRTAM$^+$, NKG2D$^+$ and
274 NKG2A/C/E$^+$ CD4$^+$GzB$^+$ T cells were severely diminished in *Myd88*$^{-/-}$ mice (**Figures**
275 **4C-4E)**. This picture does not result from lower numbers of total activated CD4$^+$ T cells
276 in infected *Myd88*$^{-/-}$ mice, as shown by the percentages and absolute numbers of CD44^{hi}
277 cells, which are equivalent to those observed in WT animals (Figure 4-figure
278 supplement 2). On the other hand, absolute numbers of CRTAM$^+$, NKG2D$^+$ and
279 NKG2A/C/E$^+$ CD8$^+$GzB$^+$ T cells were not affected in *Myd88*$^{-/-}$ mice (Figure 4-figure
280 supplement 1C-D). Concerning the expression of perforin, both the percentages and
281 absolute numbers of PRF$^+$CD4$^+$ T cells were also severely decreased in *Myd88*$^{-/-}$
282 compared to WT mice (**Figure 4F)**. The same was observed when analyzing the
283 frequency and absolute numbers of PRF$^+$CD4$^+$ T cells among GzB-expressing cells
284 (**Figure 4G)**. In order to establish to what extent the absence of MyD88 expression
285 would impact on cytotoxicity mediated by CD4$^+$ T splenocytes, we sorted activated
286 CD4$^+$CD44^{hi} T cells from both WT and *Myd88*$^{-/-}$ infected mice to a high purity level and
287 performed redirected cytotoxicity assay. Lower levels of cytotoxicity were observed
288 when sorted *Myd88*$^{-/-}$ CD4$^+$CD44^{hi} T cells were employed, as compared to assays using
289 equal numbers of sorted WT CD4$^+$CD44^{hi} T cells (**Figure 4H)**. Together, these results
290 demonstrate the important role of MyD88 signaling for the establishment of a robust
291 cytotoxic response mediated by CD4CTLs.
292
293 ***T cell-intrinsic IL-18R/MyD88 signaling plays a crucial role in the establishment of a***
294 ***CD4$^+$ T cell subpopulation bearing the CD4CTL gene signature***
295 MyD88 deficiency results in lower IL-12 production by APCs (Campos et al., 2004)
296 and this could explain the diminished numbers of CD4CTLs found in infected *Myd88*$^{-/-}$
297 mice. However, we have recently shown that IL-18R/MyD88 signaling intrinsic to

298 $CD4^+$ T cells is critical for Th1 cell proliferation and resistance to apoptosis in response
299 to infection with *T.* cruzi (Oliveira et al., 2017). If CD4CTLs herein described share a
300 common early differentiation process with (or derive from) Th1 cells, it is reasonable to
301 expect that besides IL-12 and IFN-γ, T-cell-intrinsic MyD88-dependent signaling would
302 also be important for the generation of a robust CD4CTL response. In order to test this
303 hypothesis, we constructed mix-BM chimeras in which WT (B6 x B6.SJL) F1 mice
304 were irradiated and reconstituted with a 1:1 mix of WT and *Myd88*$^{-/-}$ BM cells. After
305 reconstitution, mix-BM chimeras were infected with *T. cruzi* and, at day 14 pi, we
306 sorted WT (CD45.1) and *Myd88*$^{-/-}$ (CD45.2) $CD44^+CD4^+$ T cells to a high purity level
307 for transcriptome analysis. We then investigated whether the transcriptional signature of
308 CD4CTLs (Donnarumma et al., 2016) was present in sorted $CD4^+$ T splenocytes and to
309 what extent the absence of T-cell intrinsic MyD88-dependent signaling would impact
310 the acquirement of this transcriptional program. This signature, previously described in
311 the experimental model of Friend virus infection, distinguishes CD4CTLs from other
312 $CD4^+$ T cell subsets, including Th1 and Tfh cells (Donnarumma et al., 2016).
313 Importantly, gene set enrichment analysis (GSEA), comparing the transcriptome of
314 sorted WT and *Myd88*$^{-/-}$ $CD4^+$ T cells, revealed that 51 genes of the CD4CTL signature
315 were upregulated in WT $CD4^+$ T cells, while 78 were downregulated in *Myd88*$^{-/-}$ $CD4^+$
316 T cells (**Figures 5A-5C**). We confirmed, by flow cytometry, the upregulation of Blimp-
317 1 (*Prdm1* gene) TF and of the ecto-nucleotidase CD39 (*Entpd1*) in WT $CD4^+GzB^+$ T
318 cells (**Figures 5D** and **5E**). Of note, Blimp-1 is required for the cytotoxic function of
319 CD4CTLs (Hua et al., 2013) and CD39 expression level was found to be higher in
320 $CD4^+GzB^+$ T cells than in Tregs (**Figure 5E**).

321 In order to identify the receptor signaling upstream MyD88 responsible for the
322 establishment of a robust CD4CTL response, we further constructed three groups of

323 mix-BM chimeras, by mixing 1:1 WT and (i) *Il1r1*$^{-/-}$, (ii) *Il18ra*$^{-/-}$ or (iii) *Myd88*$^{-/-}$ BM
324 cells. A fourth group of mix-BM chimeras, 1:1 WT(B6):WT (B6.SJL) control was also
325 generated. After infection with *T. cruzi*, the percentages and absolute numbers of GzB^{+}
326 cells among CD4^{+} T lymphocytes were analyzed in each chimeric group (gate strategy
327 in Figure 5-figure supplement 1). **Figure 5F** shows that the lack of IL-18R signaling in
328 T cells, but not of IL-1R, phenocopied the absence of T cell-intrinsic MyD88 signaling,
329 revealing that IL-18R is a critical pathway upstream MyD88 necessary for the
330 establishment of the CD4^{+}GzB^{+} T cell population.

331 In order to further consolidate the role of IL-18R signaling in the generation of a
332 strong CD4CTL response, we analyzed the expression of PRF as well as of CRTAM,
333 NKG2D and NKG2A/C/E cytotoxic markers on CD4^{+}GzB^{+} T cells from the spleens of
334 *Il18ra*$^{-/-}$ mice. **Figure 6A** shows that both the frequency and absolute number of
335 PRF^{+}CD4^{+} T cells were significantly diminished in the spleens of infected *Il18ra*$^{-/-}$
336 compared to WT mice. The same was true for PRF-expressing cells among GzB^{+}CD4^{+}
337 T lymphocytes (**Figure 6B)**. As observed in infected *Myd88*$^{-/-}$ mice, the frequency of
338 GzB^{+}CD4^{+} T cells and their absolute number were also decreased in infected *Il18ra*$^{-/-}$
339 compared to WT mice (**Figures 6C-6E**). Absolute numbers of CRTAM^{+}, NKG2D^{+} and
340 NKG2A/C/E^{+} GzB^{+}CD4^{+} T cells were significantly diminished in *Il18ra*$^{-/-}$ mice as well,
341 again phenocopying results obtained in *Myd88*$^{-/-}$ mice (**Figures 6C-6E**). The cytotoxic
342 potential of CD4^{+} T splenocytes from *Il18ra*$^{-/-}$ infected animals was also evaluated by
343 performing redirected cytotoxicity assays with equal numbers of CD4^{+}CD44^{hi} T cells
344 purified from infected *Il18ra*$^{-/-}$ or WT mice. Again, as shown for *Myd88*$^{-/-}$CD4^{+} T cells,
345 lower levels of target killing were observed when employing purified *Il18ra*$^{-/-}$
346 CD4^{+}CD44^{hi} T cells as effectors (**Figure 6F**). Collectively, the present data demonstrate
347 that T-cell intrinsic IL-18R/MyD88 signaling support the generation and/or survival

348 of $CD4^+$ T cells with cytotoxic potential in response to parasite infection, revealing a
349 parallel between the requirements for the development of robust Th1 and CD4CTL
350 responses.
351
352 ***The Adoptive transfer of $CD4^+GzB^+$ T cells to $Il18ra^{-/-}$ mice extended survival to***
353 ***infection***
354 *In vivo* studies addressing the function of $CD4^+GzB^+$ T cells have been hampered by
355 the absence of a stable and abundantly expressed surface-marker of cytotoxicity, which
356 would allow purifying these cells alive. To circumvent this, we employed infected and
357 tamoxifen-treated $GzmbCreER^{T2}$/ROSA26EYFP reporter mice, from whose spleens
358 $CD4^+EYFP^+$ (GzB^+) cells were highly purified by flow cytometry and adoptively
359 transferred to infected $Il18ra^{-/-}$ mice, following the scheme shown in Figure 6-figure
360 supplement 1. The $Il18ra^{-/-}$ mouse lineage was previously shown to be very susceptible
361 to infection with *T. cruzi* (Oliveira et al., 2017), and display lower numbers of
362 $CD4^+GzB^+$ and $CD4^+PRF^+$ T cells with cytotoxic potential, as demonstrated above. The
363 transfer of highly purified $CD4^+GzB^+(EYFP^+)$ T cells to $Il18ra^{-/-}$ mice significantly
364 extended their survival rate without, however, decreasing the parasite load in the hearts
365 **(Figure 6G).** In a previous work, we have demonstrated that the transfer of total WT
366 $CD4^+$ T cells protects infected $Il18ra^{-/-}$ mice, and this property was attributed to Th1
367 cells, which are also diminished in this mouse lineage (Oliveira et al., 2017). Since
368 infected $Ifng^{-/-}$ mice have the same frequency of $CD4^+GzB^+$ T cells as WT mice in their
369 spleens (**Figure 4B**), we tested whether adoptive transfer of $CD4^+$ T cells sorted from
370 $Ifng^{-/-}$ mice would also be able to extend the survival of recipient $Il18ra^{-/-}$ mice. As
371 shown in Figure 6-figure supplement 2, this was indeed the case. Although IFN-γ
372 expression by $CD4^+$ T cells is necessary for decreasing parasitemia (Oliveira et al.,

373 2017), the present result indicated that the secretion of IFN-γ by adoptively transferred
374 $CD4^+$ T cells is not absolutely required for extending the survival time of infected
375 *Il18ra*$^{-/-}$ recipients. Together, these data demonstrate the beneficial function of the
376 $CD4^+GzB^+$ T cell subset against mortality caused by an intracellular parasite, which is
377 independent of decreasing heart parasitism.
378
379 ***The great majority of CD4$^+$ T cells in the infected myocardium express the CD4CTL***
380 ***phenotype and increased levels of immunoregulatory markers***
381 Previous studies in viral infection models suggested that CD4CTLs are present
382 in tissues where pathogen replication occurs (Marshall et al., 2017; Takeuchi et al.,
383 2016). Since *T. cruzi* heavily infects the heart, we performed intravascular staining with
384 anti-CD4 mAb and demonstrated that tissue-infiltrating $CD4^+$ T cells are abundant in
385 the myocardium of infected mice (Figure 7-figure supplement 1A-B). As shown in
386 **Figures 7A** and **7B** and Figure 7-figure supplement 2, $CD4^+GzB^+$ T cells infiltrating the
387 cardiac tissue constitute the vast majority of $CD4^+CD44^{hi}$ T cells, indicating the
388 enrichment of this subset among activated $CD4^+$ T cells in the heart compared to the
389 spleen. At the peak time-point of parasite load in the heart, $CD4^+GzB^+$ T cells in the
390 myocardium express the LAMP-1 degranulation marker at levels comparable to those
391 of $CD8^+$ T cells (**Figures 7C** and **7D** and Figure 7-figure supplement 1C). Importantly,
392 the great majority of heart-infiltrating $CD4^+GzB^+$ T cells expresses PRF, as well as the
393 CRTAM and NKG2D cytotoxic markers (**Figure 7E** and **7F)**. On the other hand, only
394 few $CD4^+GzB^+$ T cells express NKG2A/C/E in the myocardium (Figure 7-figure
395 supplement 1D, left). These data indicate a selective migration to, or retention in, the
396 infected heart of double positive $CRTAM^+NKG2D^+$ $CD4^+GzB^+$ T cells, although both
397 $NKG2A/C/E^+$ and $NKG2D^+$ cells are present at a similar ratio among $CD4^+GzB^+$ T

398 cells in the spleen. (Figure 3-figure supplement 3). On the other hand, high percentages
399 of NKG2A/C/E^{+}CD8^{+}GzB^{+} T cells were found both in the heart (Figure 7-figure
400 supplement 1D, right) and in the spleen (**Figure 3-figure supplement 4A**) of infected
401 mice.

402 We next investigated the ratio of cells expressing the immunoregulatory markers
403 Lag-3, Tim-3, CD39 and PD-1 among different CD4^{+} T cell subsets of infected mice:
404 naïve cells (CD44^{lo}GzB^{-}PRF^{-}), activated non-cytotoxic (CD44^{hi}GzB^{-}PRF^{-}) or activated
405 cytotoxic (CD44^{hi}GzB^{+}PRF^{+}) cells. The intensity of expression of these markers in each
406 cell subpopulation was also analyzed. Results in **Figure 7-figure supplement 3,** show
407 that CD44^{hi}GzB^{+}PRF^{+} CD4^{+} T cells compose the subset of activated cells among which
408 the higher frequencies of cells expressing these markers are found, both in the spleen
409 and in the heart, at day 14 pi. The only exception was the equal ratio of cells expressing
410 PD-1, at equivalent levels, when comparing splenic CD44^{hi}GzB^{-}PRF^{-} and
411 CD44^{hi}GzB^{+}PRF^{+} CD4^{+} T cells. Similarly, equivalent percentages of cells expressing
412 PD-1 among CD44^{hi}GzB^{-}PRF^{-} and CD44^{hi}GzB^{+}PRF^{+} CD4^{+} T cells were found in the
413 heart. However, the intensity of expression of the PD-1 marker was significantly higher
414 among CD44^{hi}GzB^{+}PRF^{+} (CD4CTLs) compared to CD44^{hi}GzB^{-}PRF^{-} CD4^{+} T cells
415 infiltrating the cardiac tissue. Furthermore, we analyzed whether these parameters differ
416 between CD4CTLs in the spleen and in the heart (**Figure 7-figure supplement 4)**. Of
417 note, while MFI values of Tim-3, CD39 and PD-1 expression were increased on
418 CD4CTLs in the heart compared to CD4CTLs in the spleen, Lag-3 expression levels
419 were decreased on CD4CTLs infiltrating the myocardium. Furthermore, only the
420 expression of PD-1, but not of Lag-3, Tim-3 or CD39, is upregulated on CD8CTLs in
421 the heart compared to the spleen (**Figure 7-figure supplement 4)**, an indication that the

422 *T. cruzi*-infected cardiac tissue is a less so-called exhaustion-inducing environment
423 compared to certain tumors.
424
425 ***The frequency of CD4$^+$PRF$^+$ T cells correlates with cardiomyopathy in Chagas***
426 ***patients***
427 Finally, we investigated the presence of PRF$^+$CD4$^+$ T cells in the circulation of
428 patients infected with *T. cruzi* and suffering from chronic Chagas cardiomyopathy (CC).
429 In order to ascertain the specificity of CD4$^+$ T cells against *T. cruzi*, PBMC from CC
430 patients or from healthy donors (HD) were incubated (or not) with trypomastigote-
431 derived antigens (trypo) and analyzed for the expression of perforin by flow cytometry
432 (**Figure 7-figure supplement 5**). As shown in **Figures 7G** and **7H,** after incubation
433 with trypo, both the expression level of PRF (MFI) and the percentage of PRF$^+$CD4$^+$ T
434 cells increased among CD4$^+$ T cells from CC patients, but not from HD controls. Of
435 note, CD4$^+$ T cells expressing PRF were found at higher frequency in CC patients than
436 in HD (**Figure 7I)**. We next performed correlative analyses between the frequency of
437 PRF-expressing CD4$^+$ T cells in PBMC from CC patients and two echocardiographic
438 parameters, usually employed to evaluate cardiac function in CC patients: left
439 ventricular ejection fraction (LVEF) and left atrium diameter. As shown in **Figure 7J,** a
440 clear inverse correlation between the frequency of CD4$^+$PRF$^+$ T cells and LVEF, as
441 well as a direct correlation between the frequency of these cells and the left atrium
442 diameter was found. These correlations suggest that CD4CTLs might play a pathogenic
443 role in the chronic phase of Chagas disease, although the alternative possibility remains
444 that the higher levels of CD4CTLs reflect elevated parasite burden and/or inflammation
445 in the heart, without a direct involvement of this cell subset in the pathology. Together,
446 data obtained here in CC patients and in the mouse experimental model point to the

447 heart as an important target-organ for $CD4^+$ T cells with cytolytic potential generated in
448 response to infection with *T. cruzi.*
449
450 **Discussion:**
451 Here we show for the first time that CD4CTLs are abundantly present in the
452 spleen of mice infected with *T. cruzi* and that such phenotype predominates among
453 $CD4^+$ T cells infiltrating the infected cardiac tissue. The expression of LAMP-1
454 degranulation marker by $CD4^+GzB^+$ T cells in the heart and in the spleen indicates that
455 these cells may play important effector functions in both organs. $GzB^+PRF^+CD4^+$ T
456 cells present in the *T. cruzi*-infected hearts express CRTAM and NKG2D cytotoxicity
457 markers, but differently from CD4CTLs found in the lungs of mice infected with IAV
458 (Marshall et al., 2017), do not express NKG2A/C/E molecules. This interesting
459 dissimilarity requires further investigation and could be due to differential regulation
460 exerted by tissue-specific factors or, alternatively, by different innate responses
461 influencing CD4CTL differentiation, which would be distinctly triggered by viral and
462 parasite pathogens.
463 $CD4^+$ T cells purified from the spleen of infected mice killed APCs presenting
464 parasite-derived antigens *in vitro,* in a GzB- and PRF-dependent process. *In vivo* Ag-
465 specific cytotoxicity against parasite-derived I-A^b-restricted epitopes was also observed.
466 It is expected that killing of infected APCs in the spleen should lead to a decrease in the
467 activation of effector T cells, dampening the exuberant immune response against the
468 parasite. Therefore, the cytotoxic action of CD4CTLs may contribute to
469 immunoregulation, avoiding the development of exacerbated immunopathology that can
470 cause mortality in the acute phase of the infection with *T. cruzi.* Favoring this
471 hypothesis, we showed that adoptive transfer of $CD4^+GzB^+$ T cells to susceptible

472 *Il18ra*$^{-/-}$ mice, which have lower levels of these cells, significantly increased their
473 survival to infection without, however, affecting parasite loads. The incapacity of
474 transferred CD4CTLs in decreasing parasite loads in the heart might be due to two
475 facts: (i) cytotoxicity mediated by CD4CTLs is MHC class II-restricted, but only heart
476 endothelial cells express MHC class II molecules, while the infected cardiac muscle
477 cells remain MHC II-negative (Reis et al, 1993); (ii) as shown here, only a small
478 fraction of CD4^{+} T cells with cytolytic phenotype produce IFN-γ, the main cytokine
479 inducing trypanosomicidal function in macrophages and cardiomyocytes (Machado et
480 al., 2000). Accordingly, adoptive transfer of highly purified *Ifng*$^{-/-}$ CD4^{+} T cells (among
481 which the same frequency of GzB^{+} cells were found) also resulted in the significantly
482 increase of the survival time of infected *Il18ra*$^{-/-}$ mice, but did not decrease parasite
483 levels (Oliveira et al., 2017). The data discussed above, along with the fact that the
484 parasite load is not decreased in the recipient mice indicate that IFN-γ is not involved in
485 the extended survival granted by adoptive transfer of CD4^{+}GzB^{+} T cells and exclude a
486 role for Th1 cells, which are known to exert an important microbicidal function through
487 the production of IFN-γ (Oliveira et al., 2017). Together with our previous work, the
488 current results point to complementary roles exerted by CD4CTL and Th1 cells. Both
489 cell types might be required for survival against infection with *T. cruzi*, working
490 together to establish a balance between the Th1-dependent control of parasite load on
491 one side, and CD4CTL-mediated dampening of the immunopathology resulting from
492 this process, on the other. In fact, it is known that IFN-γ plays a central but dual role in
493 Chagas disease, having both important microbicidal and pathogenic functions (Ferreira
494 et al, 2014). The equilibrium between anti-parasitic and anti-inflammatory responses
495 underlies the establishment of the asymptomatic form of chronic infection (Nunes et al.,
496 2018), in which increased levels of CD4^{+}GzB^{+} T cells have been found in humans

497 (Keesen et al., 2012). Therefore, our results are in accordance with an
498 immunoregulatory role played by CD4CTLs, likely through the GzB/PRF/FasL-
499 mediated killing of infected APCs in an IFN-γ-independent manner, although it is not
500 possible to formally attribute the beneficial role of adoptively transferred CD4CTLs
501 exclusively to their cytolytic action.

502 Of note, we also show here that most $CD4^+GzB^+PRF^+$ T cells express surface
503 co-inhibitory receptors, such as Lag-3 and Tim-3, as well as the ecto-ATPase CD39, at
504 particularly high levels. These regulatory molecules, typically expressed by Treg, Tr1
505 cells and terminally differentiated or exhausted $CD8^+$ or $CD4^+$ T cells, have been
506 implicated in the immunoregulatory functions of these cell subsets (Anderson et al.,
507 2016; Mascanfroni et al., 2015; Park et al., 2019). Although almost the totality of
508 $CD4^+GzB^+$ T cells express T-bet, only a minority of these cells produce IFN-γ. Most
509 $CD4^+GzB^+$ T cells also express Eomes and/or Blimp-1, two transcription factors which
510 are known to be involved in T cell exhaustion. Whether the repression of IFN-γ in
511 $CD4^+GzB^+$ T cells is mediated by Eomes and/or Blimp-1, as evidentiated in $CD4^+$ T
512 cells during infection with *Toxoplasma gondii* (Hwang, et al., 2016), remains to be
513 determined. Thus, the phenotype of a large fraction of $CD4^+GzB^+PRF^+$ T cells
514 developing in response to infection with *T. cruzi* is typical of terminal
515 differentiated/exhausted cells. Nevertheless, it is important to note that highly functional
516 effector T cells can also express inhibitory receptors and despite exhaustion being often
517 seen as a dysfunctional state, it has been shown that the expression of inhibitor
518 molecules allows T cells to persist and to contribute to the contention of chronic viral
519 infections without causing immunopathology (reviewed in Wherry, 2011).

520 Chronic Chagas cardiomyopathy usually develops in around 30% of infected
521 individuals after decades, probably reflecting an imbalance between parasite and host

522 immune response (Nunes et al., 2018). Although the exact mechanism remains to be
523 elucidated, the association of NK, CD8CTL and GzA-expressing $CD4^+$ T cells with the
524 development of chronic carditis has been indicated (Ferreira et al., 2017; Menezes et al.,
525 2012; Nunes et al., 2018). Since CD4CTLs recognize the cognate antigen in the context
526 of MHC class II molecules, the lysis of infected MHC II^+ endothelial cells in the heart
527 might trigger immunopathology in the chronic phase, in contrast to the possible
528 immunoregulatory role due to the killing of infected APCs in the spleen, during the
529 acute phase of infection, as discussed above. In the present study, we found that the
530 frequency of parasite-specific $CD4^+PRF^+$ T cells is increased in the blood of chronic
531 cardiac patients with Chagas disease (CC) when compared to healthy donors. A
532 correlation between the frequency of PRF^+CD4^+ T cells and two echocardiographic
533 parameters employed for evaluating myocarditis in CC patients was also encountered. It
534 is tempting to speculate that the loss of regulatory function exerted by different $CD4^+$ T
535 cell subsets, including CD4CTLs, might lead to the chronic pathology. Alternatively,
536 the increased levels of CD4CTLs in chronic patients might be reflecting parasite burden
537 and/or tissue inflammation without exerting a pathogenic function. Therefore, further
538 studies are necessary for fully defining the role of tissue-infiltrating CD4CTLs in
539 Chagas disease. Interestingly, NKG2D, expressed by most CD4CTLs in the heart, can
540 mediate both activating and inhibitory signals (Wensveen et al., 2018). Importantly, a
541 polymorphism in one of the NKG2D ligands, the major histocompatibility complex
542 class I–related chain A gene (MICA) molecule, was associated with left ventricular
543 systolic dysfunction in patients with chronic Chagas myocarditis (Ayo et al., 2015).

544 We have shown here that $CD4^+GzB^+$ T cells originating in response to *T. cruzi*
545 infection largely outnumber IFN-γ-producing $CD4^+$ T cells and that their appearance in
546 the spleen follows the same kinetics of classic Th1 cells, indicating thereby that

547 differentiation of CD4CTLs is not a late event during infection. Of note, more than 60%
548 of $CD4^+GzB^+$ T cells have downregulated CD27 expression in the spleen at day 14 pi, a
549 characteristic of terminally differentiated T cells (Takeuchi & Saito, 2017). We have
550 also shown here that the majority of $CD4^+GzB^+$ T cells express T-bet, Eomes and
551 Blimp-1. Although Eomes seems not to be essential for CD4CTLs in certain studies
552 (Donnarumma et al., 2016; Kotov et al., 2018), it was proposed to be the master
553 regulator for CD4CTLs and Tr1 cells by others (Curran et al., 2013; Eshima et al., 2012;
554 Qui et al., 2011; Zhang et al., 2017). The $CD4^+GzB^+$ T cell population described herein
555 presents some characteristics in common with Tr1 cells. However, we only detected a
556 very low frequency of $CD4^+GzB^+$ T cells co-expressing Lag-3 and CD49b (Gagliani et
557 al., 2013) or IL-10. In this regard, data from *T. cruzi* infection differs from those
558 observed during infection with other intracellular parasites such as *T. gondii* and certain
559 *L. major* strains, in which high frequencies of $CD4^+$ T cells producing both IL-10 and
560 IFN-γ were described (Anderson et al., 2007; Jankovic et al., 2007). In contrast with
561 ThPOK-negative CD4CTLs that accumulate in the gut (Cheroutre & Husain, 2013;
562 Mucida et al., 2013; Reis et al., 2013), $CD4^+GzB^+$ T cells in the *T. cruzi*-infected spleen
563 express ThPOK at the peak of infection. Interestingly, the absence of ThPOK
564 downregulation was also observed in mouse (Mittal et al., 2018) and human CD4CTLs
565 (Serroukh et al., 2018). Thus, different subsets of CD4CTL possibly exist, in which the
566 interplay between ThPOK and RUNX3 expression might be differentially regulated.

567 Although many authors consider CD4CTLs merely functional variants of Th1 cells,
568 in some models CD4CTLs fail to fit Th1-defining criteria, such as the dependence on
569 IL-12, STAT4 or T-bet for differentiation (Brown et al., 2009; Curran et al., 2013; Hua
570 et al., 2013; Kotov et al., 2018). Nonetheless, in agreement with other studies (Cooper et
571 al., 2004; Krueger et al., 2021; Tagawa et al., 2016; Xie et al., 2010), we showed here

572 that $CD4^+GzB^+$ T cells are scarcely generated in the absence of IL-12p40. Importantly,
573 we demonstrated that the expansion/survival of CD4CTLs also depends on T-cell
574 intrinsic IL-18R/MyD88 signaling, which we have previously shown to induce cell
575 cycling, anti-apoptotic and Th1-signature transcripts (Oliveira et al., 2017). Notably,
576 several genes of the CD4CTL signature, which distinguishes this subset from Th1 and
577 Tfh cells (Donnarumma et al., 2016), were expressed by WT, but not by *Myd88*$^{-/-}$ $CD4^+$
578 T cells from infected mix-BM chimeras. Therefore, analogous to its action on Th1 cells,
579 we showed here that T-cell intrinsic IL-18R/MyD88 signaling contributes for the
580 reinforcement and/or stabilization of $CD4^+$ T cell commitment into the CD4CTL
581 phenotype. IFN-γ is another key cytokine involved in Th1 differentiation and *Ifng*$^{-/-}$
582 mice are extremely susceptible to infection with *T. cruzi* (Campos et al., 2004).
583 Interestingly, we found no difference in the frequency of $CD4^+GzB^+$ T cells between
584 WT and *Ifng*$^{-/-}$ infected mice, in accordance with a study showing that IFN-γ had no
585 impact on the ability of CD4 effectors to acquire cytolytic activity (Brown et al., 2012).
586 However, both GzB^+ and total $CD4^+$ T-cell numbers were significantly lower in the
587 infected *Ifng*$^{-/-}$ animals, indicating that IFN-γ might also play a role in the
588 expansion/survival of both Th1 and CD4CTLs in our system. It is known that IFN-γ and
589 IL-18R participate in a reciprocal positive feedback loop in Th1 differentiation process:
590 while IFN-γ is required for IL-12-driven upregulation of IL-18R expression (Nakahira
591 et al., 2001; Smeltz et al., 2001), IL-18 is a major IFN-γ-inducing factor. Therefore, the
592 absence of IL-18R upregulation in $CD4^+$ T cells of *Ifng*$^{-/-}$ mice would prevent the
593 expansion of both $CD4^+$ T cell subpopulations. Thus, in *T. cruzi* infection model, IL-12,
594 IFN-γ and IL-18R/MyD88 signaling act as key pathways at early check-points in the
595 generation of $CD4^+GzB^+$ T cells with cytotoxic potential, suggesting that these cells

596 might share common early differentiating steps with the Th1 subset. It is not excluded,
597 however, that different precursors of CD4CTL and Th1 cells might exist (Takeuchi &
598 Saito, 2017). A cartoon summarizing our results and cited works published by others is
599 shown in Figure 7-figure supplement 6. Of note, in humans, the higher production of
600 IL-18 due to gene polymorphisms has been correlated to protection against chronic
601 Chagas cardiomyopathy (Leon Rodriguez et al., 2016; Nogueira et al., 2015).

602 It is possible that differentiation into CD4CTLs could also be influenced by
603 pathogen-derived factors. Very recently, Krueger *et al*. have shown that a subset of IL-
604 12-dependent Th1-derived cytotoxic cells was present in the spleen of *Il18*$^{-/-}$ mice at
605 later stages of infection with *Salmonella enterica* (Krueger et al., 2021). Whether that
606 result was due to compensatory mechanisms, such as the known exacerbated IL-12
607 production by infected *Il18*$^{-/-}$ mice (Monteforte et al., 2000), or to distinct innate
608 responses, differentially induced by phagosomal bacteria and cytosolic parasites,
609 remains to be determined. Of note, other discrepancies between results obtained with
610 *Il18*$^{-/-}$ versus *Il18ra*$^{-/-}$ mouse lineages have been described in different models in the past
611 (Gutcher et al., 2006; Lewis & Dinarello, 2006). It is known that different classes of
612 pathogens can trigger diverse APC responses and, therefore, elicit pathogen-tailored Th
613 programs (Kara et al., 2014; Kiner et al., 2021). Previous works have reported the
614 immunoregulatory action of *T. cruzi*-derived PAMPs on CD4^{+} T cell activation, either
615 by directly acting as co-stimulatory signals for T cells, or by modulating APC functions
616 (Bellio et al., 1999; DosReis et al., 2002; Medeiros et al., 2007). It would be interesting
617 to test *T. cruzi*-derived molecules on their capacity to favor the generation of CD4CTLs.

618 In summary, the present work is the first to describe a CD4CTL subset abundantly
619 present in the *T. cruzi*-infected cardiac tissue, bringing novel pieces to the scenario of
620 the immune response against a major human intracellular parasite. Importantly, our

621 data disclose a mechanistic framework involved in the generation of a robust CD4CTL
622 response, whose control and optimization may provide new therapeutic and vaccination
623 strategies to combat infection with intracellular pathogens and chronic diseases
624 resulting thereof.
625

626 **Materials and Methods**

627 **Mice.** C57BL/6, B6.SJL and F1 (B6 x B6.SJL) mice were from the Universidade
628 Federal Fluminense. *Myd88*$^{-/-}$ mice were generated by Dr. S. Akira (Osaka University,
629 Japan); *Il12p40*$^{-/-}$ and *Ifng*$^{-/-}$ mice were purchased from USP; *Il18ra*$^{-/-}$ and *Il1r1*$^{-/-}$ mice
630 from JAX Mice, USA. GzB reporter mice, GzmbCreER^{T2}/ROSA26EYFP, previously
631 described (Bannard et al., 2009) were provided by Dr. Ricardo Gazinelli (UFMG, BH,
632 Brazil). Mice were on the C57BL/6 background, except GzmbCreER^{T2}/ROSA26EYFP,
633 which were on mixed Sv129/B6 background and backcrossed to B6 for 5 generations.
634 In each experiment, only male mice of the same age (6- to 8-week-old) were used. Mice
635 were housed at a maximum of 5 animals per cage, in forced-air-ventilated micro-
636 isolation rack system, in a room at 21–23˚C under a 12/12 h light/dark cycle and
637 provided with sterilized water and chow ad libitum. All mouse experiments were
638 conducted in accordance with guidelines of the Animal Care and Use Committee of the
639 Federal University of Rio de Janeiro (Comitê de Ética do Centro de Ciências da Saúde
640 CEUA - CCS/UFRJ, license: IMPPG022).

641 **Experimental infection.** Bloodstream trypomastigotes of the Y strain of *T. cruzi* (2 x
642 10^3 cells/0.2 mL) were inoculated intraperitoneally (i.p.). Y-OVA strain trypomastigotes
643 (Gomes-Neto et al., 2018) were obtained from LLC-MK2 infected cultures and 2 x 10^6
644 trypomastigotes (in 0.2 mL PBS) were inoculated i.p. Rare outliers (mice in which the
645 infection was not properly established) were identified by the lower size of the spleen

646 (total cell number) and lower percentage of $GzB^{+}CD8^{+}$ T cells (inferior of 50%) in the
647 spleen. These outlier mice were excluded from all analyses. Mice found at the moribund
648 condition (presenting unambiguous signals that the experimental endpoint has been
649 reached), were euthanized.

650 **Generation of BM chimeras.** Acidic drinking water (pH 2.5-3.0) was given for 8 days
651 to recipient mice prior to irradiation with a lethal single dose of 800 rad (TH780C -
652 Theratronics, Canada). The day after irradiation, BM cells were transferred and mice
653 were treated with neomycin sulfate (2 mg/mL) in the drinking water for 15 days.
654 Marrow was harvested from the femur and tibia of B6.SJL ($CD45.1^{+}$) and B6, *Myd88*$^{-/-}$,
655 *Il1r1*$^{-/-}$ or *Il18ra*$^{-/-}$ ($CD45.2^{+}$) mice. For mixed BM chimeras, $CD45.1^{+}$ and $CD45.2^{+}$ BM
656 cells were transferred in a 1:1 ratio (2 x 10^{6} cells each) to irradiated mice. In all
657 experiments, mice were infected 6 to 8 weeks after cell transfer, when reconstitution
658 was achieved.

659 **Human population.** A total of thirteen volunteers were enrolled in this study. Nine
660 volunteer patients had positive specific serology for *T. cruzi* and displayed the chronic
661 Chagas cardiomyopathy (CC) with right and/or left ventricular dilation, global left
662 ventricular dysfunction, alterations in the cardiac electric impulse generation and
663 conduction upon electrocardiogram, chest x-rays and echocardiography; four
664 individuals displayed negative specific serological tests for Chagas disease and were
665 included as control group (healthy donors, HD). Patients were from Chagas disease
666 endemic regions within Minas Gerais, Brazil, and were evaluated at the outpatient clinic
667 of the Universidade Federal de Minas Gerais. Healthy donors were from Belo
668 Horizonte, which is a non-endemic region for Chagas disease. We excluded from our
669 study individuals with any other chronic inflammatory diseases, diabetes,
670 heart/circulatory illnesses or bacterial infections. All individuals included in this work

671 were volunteers and treatment and clinical care were offered to all patients, as needed,
672 despite their enrollment in this research project. All participants provided written
673 informed consent for participation in the study. This cross-sectional study is part of an
674 extended project evaluating biomarkers of cardiomyopathy development in Chagas
675 disease, which has the approval of the National Committee of Ethics in Research
676 (CONEP#195/2007) and are in accordance with the Declaration for Helsinki.

677 **PBMC flow cytometry.** Peripheral blood samples were collected in heparin tubes.
678 PBMCs were obtained by separating whole blood over Ficoll (Sigma-Aldrich, St.
679 Louis, MO), as previously described (Menezes et al., 2012). Cells were washed and
680 resuspended in RPMI 1640 medium (Gibco, Rockville, MD) supplemented with 5%
681 heat-inactivated AB human serum, antibiotics (penicillin, 200 U/ml; and streptomycin,
682 0.1 mg/mL) and L-glutamine (1 mM) (Sigma-Aldrich) at a concentration of 1 x 10^7
683 cells/mL. Cells from each volunteer were cultured on 96-well plates (Costar, Corning
684 Incorporated, Corning, NY) in 200 µL of medium alone (ctr) or containing 20 µg/mL of
685 trypomastigote antigen (trypo) for 18h. Trypo was obtained from trypomastigotes
686 purified from VERO cell cultures: parasites were washed, freeze-thawed for 3 cycles,
687 followed by 5 cycles of 5 minutes each of sonication using 30 seconds between them.
688 Samples were ultracentrifugated at 5,000g for 60 min, at 4^oC. Supernatants were
689 collected, dialyzed for 24h and protein quantification performed by Bradford method.
690 Cells (2 x 10^5) were incubated with PerCP-anti-CD4 (clone A161A1) antibody
691 (Biolegend) for 15 min at 4°C, washed in phosphate-buffered saline (PBS) containing
692 1% bovine serum albumin (BSA), and fixed by a 20 min incubation with a 2%
693 formaldehyde. After washing with PBS, cells were permeabilized with 0.5% saponin
694 for 15 min and intracellularly stained with PE-anti-perforin (clone B-D48) antibody
695 (Biolegend) for 20 minutes, washed twice with 0.5% saponin solution, resuspended in

696 PBS and analyzed. A minimum of 100,000 gated events from each sample were
697 collected and analyzed using FlowJo software.
698 **Flow cytometry of mouse cells.** Reagents and antibodies: PB-anti-CD45.1, APC-Cy7-
699 anti-CD45.2, FITC- PE- or BV-605-anti-CD4, PE-anti-CD8, PE-Cy7-anti-NK1.1,
700 BV421-anti-TCRβ, PE-anti-2B4, FITC-anti-CD107a, PE-Cy7-anti-CD39, PE-anti-
701 FasL, PE-Cy7-anti-CRTAM, PE-anti-NKG2D, PE-anti-NKG2A/C/E, FITC- or
702 AlexaFluor647-anti-GzB, PE-anti-Eomes, PE- or A647-anti-T-bet, PE-anti-FoxP3,
703 AlexaFluor647-anti-Blimp1 and PE-anti-PRF were used. All mAbs were purchased
704 from Biolegend, BD Biosciences or eBioscience/Thermo Fisher Scientific. Spleen cells
705 were stained after red blood cell lysis with ACK buffer. Hearts were perfused with 20
706 mL of cold PBS, minced into small fragments and treated with collagenase D (1.0
707 mg/mL) and DNAse I (0.1 mg/mL), for 1 hour at 37ºC. Collagenase D, DNAse I,
708 monensin and saponin were purchased from Sigma-Aldrich. Single cell suspensions
709 were incubated with anti-CD16/CD32 (FcR block) for 5 min and then surface stained
710 for 30 min on ice. For IL-10 and IFN-γ intracellular staining, 2 x 10^6 spleen cells were
711 cultured in the presence of PMA (16 nM), ionomycin (0.5 μM), monensin (5 μM) and
712 brefeldin A (3.0 μg/mL) for 4 hours. After staining for surface markers, cells were fixed
713 with paraformaldehyde 1% for 1 h, permeabilized with saponin 0.2% for 20 min and
714 stained with PE-Cy7-anti-IFN-γ mAb and/or PE-anti-IL-10 mAbs (Biolegend). For TF
715 and GzB/PRF staining, the FoxP3 staining buffer kit (eBioscience, ThermoFisher
716 Scientific) was employed. At least 20,000 events gated on $CD4^+$ T cells were acquired.
717 Analytical flow cytometry was conducted with MoFlo (Beckman Coulter/Dako-
718 Cytomation), FacsCanto, FacsCalibur or BD LSRFortessa (BD Bioscience) and data
719 analyzed with Summit V4.3 software (Dako Colorado, Inc).

720 ***In vitro* and *in vivo* cytotoxicity assays.** For redirected cytotoxic assay, sorted B cells
721 ($B220^+$), previously activated by LPS (InvivoGen), at 25 μg/ml for 48 h and then
722 incubated for 1 h with anti-CD3ε antibody (10 μg/mL), were employed as target cells.
723 FACS-sorted naïve ($CD44^{low}CD4^+$) and effector/memory ($CD44^{hi}CD4^+$) T cells were
724 purified from the spleen of non-infected and infected mice, respectively. In some
725 experiments, sorted T cells were treated for 1 h with GzB (Z-AAD-CMK, 10 μM) and
726 PRF (Concamycin A, 0.5 μM) inhibitors (Biovision Inc., Milpitas, CA), before
727 coincubation at different E:T ratios, with 10^4 target B cells (prepared as
728 aforementioned) in round-bottom microplates (Costar-Corning) for 14 h, at 37ºC in a
729 5% CO_2 incubator and in triplicates. After incubation, living target cells were quantified
730 by flow cytometry, after staining with propidium iodide at 0.5 μg/ml (Sigma-Aldrich).
731 For *T. cruzi*-specific cytotoxicity assays, $CD4^+$ T cells were obtained from infected B6
732 mice, at day 14 pi, and purified by FACS sorting (MoFlo cell sorter, Beckman
733 Coulter/Dako-Cytomation). IC-21 macrophage cell lineage (ATCC) were used as
734 targets *in vitro.* For this, IC-21 cells were counted and split into two tubes: half of the
735 target cells were incubated for 45 min at 37º C in 5% CO_2, in RPMI containing *T. cruzi*
736 amastigote protein extract (30 μg/mL) obtained as previously described (Oliveira et al.,
737 2010). Ag-loaded cells were then stained with 2.5 μM CFSE ($CFSE^{Hi}$) (Invitrogen, Life
738 Technologies), and control cells with 0.5 μM CFSE ($CFSE^{Low}$) in 5 mL of warm PBS
739 for 10 min at 37º C. After two washes in RPMI 1640 (10% FCS), cells were
740 resuspended at a concentration of 2 x 10^5 cells/mL each and mixed at 1:1 ratio
741 ($CFSE^{Hi}$:$CFSE^{Low}$). Purified $CD4^+$ T cells were added at different E:T ratios. Cells were
742 seeded in duplicate to round-bottom 96-well plate in a final volume of 200 μL. After
743 ON incubation, cells were harvested, incubated with 0.5 μg/mL of propidium iodide and

744 PI^+ cells were excluded from FACS analysis. The percentage of specific lysis was
745 calculated using the formula: % of specific lysis = 100x [($CFSE^{Low}$ / $CFSE^{Hi}$) ctr −
746 ($CFSE^{Low}$ / $CFSE^{Hi}$) effector] x ($CFSE^{Low}$ / $CFSE^{Hi}$) ctr^{-1}. For *in vivo* cytotoxicity
747 assays, splenocytes from non-infected B6 mice were employed as target cells after
748 being divided in 3 subpopulations and stained with 10.0 (High), 2.5 (Int) and 0.625
749 (Low) μM of CFSE or of CTV (Invitrogen, Life Technologies). $CFSE^{Int}$ and $CFSE^{Low}$
750 cells were loaded with one of the following peptides: SA85c (SHNFTLVASVIIEEA),
751 SA85d (LVASVIIEEAPSGNT), $OVA_{323-339}$, $OVA_{257-263}$ or PA8 (VNHRFTLV) at 2
752 μM, all from GenScript, EUA. $CFSE^{Hi}$ cells were not loaded with any peptide and used
753 as internal control. For calculating the percentage of specific lysis, $CFSE^{Hi}$ and $CFSE^{Int}$
754 (or $CFSE^{Low}$) were gated together in order to constitute 100% of cells. $CFSE^{Hi}$ and
755 $CFSE^{Int}$ (or $CFSE^{Low}$) populations were then individually gated and specific lysis was
756 calculated using the following formula: % of specific lysis = 100x [($CFSE^{Low\ or\ Int}$ /
757 $CFSE^{Hi}$) ctr − ($CFSE^{Low\ or\ Int}$ / $CFSE^{Hi}$) effector] x ($CFSE^{Low\ or\ Int}$ / $CFSE^{Hi}$) ctr^{-1}.
758 **Real time RT-PCR.** RNA was extracted using the RNeasykit (QIAGEN). cDNA was
759 synthesized using the High Capacity cDNA Reverse Transcription Kit (Invitrogen, Life
760 Technologies), following the manufacturer's instructions. Gene expression was
761 analyzed using primers in combination with SYBR Green® on a StepOneReal Time
762 PCR System (Applied Biosystems, Life Technologies). The expression level of the
763 genes of interest was determined relative to the expression of 18S rRNA. Primers:
764 *Runx3* Fwd.: 5'- ACA GCA TCT TTG ACT CCT TCC -3'; *Runx3* Rev.: 5- GTT GGT
765 GAA CAC GGT GAT TG- 3'; *Thpok* Fwd: 5'- ATG GGA TTC CAA TCA GGT CA-
766 3'; *Thpok* Rev.5'- TTCTTC CTA CAC CCT GTG CC -3'; *CD8a* Fwd: 5' - ACT GCA
767 AGG AAG CAA GTG GT – 3'; *CD8a* Rev: 5'-CAC CGC TAA AGG CAG TTC TC-
768 3'; 18S-Fwd.: 5'- GGG CGT GGG GCG GAG ATA TGC - 3' and 18S-Rev.: 5'- CG

769 CGG ACA CGA AGG CCC CAA A -3'. For parasite load quantification, hearts of
770 infected mice were perfused, minced and immediately homogenized in 1.0 ml of 4.0 M
771 Guanidine thiocyanate (SIGMA-Aldrich) containing 8.0 μl/mL of β-mercaptoethanol
772 and processed for DNA extraction. Generation of PCR standards and detection of
773 parasite tissue load by real-time PCR was carried out as described (Oliveira et al.,
774 2017); briefly, primers amplify a repeated satellite sequence of *T. cruzi* DNA of 195
775 base-pairs: TCZ-Fwd.: (5'-GCTCTTGCCCACAAGGGTGC-3') and TCZ-Rev.: (5'-
776 CCAAGCAGCGGATAGTTCAGG-3'). Reactions with TNF-a-Fwd: (5'-
777 CCTGGAGGAGAAGAGGAAAGAGA-3') and TNF-a-Rev.: (5'-
778 TTGAGGACCTCTGTGTATTTGTCAA-3') primers for *Mus musculus* TNF-α gene
779 were used as loading controls.

780 **Gene-expression analysis.** Gene expression data were extracted with GeneSpring
781 software GX 11.0 software using default parameters. Data were then normalized by
782 subtracting the average from all genes from each gene intensity and dividing the result
783 by the standard deviation of all gene intensities (i.e. z-score normalization). Z ratios
784 were calculated as previously described (Cheadle et al., 2003) and used to compare the
785 difference in expression between WT samples and *Myd88*$^{-/-}$ samples. Gene Set
786 Enrichment Analysis (GSEA) (http://www.broadinstitute.org/gsea/index.jsp) was
787 performed on the genes pre-ranked by Z ratios (1,000 permutations and Weighted
788 Enrichment Statistic) using as data set 82 differentially expressed genes of sorted WT
789 and *Myd88*$^{-/-}$CD4^{+} T cells (GEO accession no. GSE57738) (Oliveira et al., 2017); and
790 using as gene set the CD4^{+}GzmB^{+} (CD4CTL) transcriptional signature (159 upregulated
791 genes) previously described (https://www.ebi.ac.uk/ena/data/view/PRJEB14043).

792 **Adoptive CD4^{+} T cell transfer assay.** Eight-week-old male
793 GzmbCreER^{T2}/ROSA26EYFP mice were infected with 2 x 10^{3} trypomastigotes and

794 treated with 4 mg/animal/day of tamoxifen citrate (Sandoz-Novartis) from day 7 to 11
795 pi by gavage. Spleen cells were harvested and treated with ACK for red blood cells lysis
796 at day 13 pi. Alternatively, $CD4^+$ T cells were purified from the spleen of non-treated
797 and infected *Ifng*$^{-/-}$ mice. In both cases, spleen cells were labeled with biotinylated anti-
798 B220, anti-CD11b, anti-NK1.1, anti-γδTCR, anti-CD8 and PE-conjugated anti-CD4
799 antibodies for 30 minutes on ice, followed by staining with PE-Cy7-conjugated
800 Streptavidin for 20 min. Residual PE-Cy7$^+$ cells were excluded and $EYFP^+PE^+$
801 ($CD4^+GzB^+$ T cells) or PE^+CD4^+ (*Ifng*$^{-/-}$$CD4^+$ T cells) were sorted using MoFlo cell
802 sorter (Beckman Coulter/Dako-Cytomation). $CD4^+GzB^+$ T cells (2.8 x 10^5 cells/animal)
803 or *Ifng*$^{-/-}$ $CD4^+$ T cells (1.3 x10^6 cells/animal), both presenting purity higher than 98%,
804 were adoptively transferred by *iv* injection into *Il18ra*$^{-/-}$ recipient mice, previously
805 infected with 1 x 10^3 trypomastigotes (day 7 pi). Control groups of *Il18ra*$^{-/-}$ and *Myd88*$^{-}$
806 $^{/-}$ infected mice received PBS. Survival was accompanied daily.
807 **Statistics.** Statistical analyses were performed using GraphPad Prism version 6 for Mac
808 OS (GraphPad Software, San Diego California USA, www.graphpad.com). Sample
809 sizes were chosen to allow the detection of statistical differences with $p < 0.5$ using
810 Student's *t* test, or the Log-rank (Mantel-Cox) test for mouse survival curves.
811 Correlation analysis employed Pearson correlation test. When comparing two groups,
812 the minimum number was n=3 per group. In some experiments, the number was
813 increased to n= 9 to permit $p < 0.05$ even considering the possibility of a single outlier
814 in a population. Data are expressed as mean $\pm$ SEM and considered statistically
815 significant if *p* values were < 0.05.
816

Acknowledgments:

General: We would like to thank Dr. Ricardo T. Gazzinelli (Fiocruz, MG, Brazil) for enriching discussion and providing GzmbCreER^{T2}/ROSA26EYFP mouse lineage, Dr. Helder I. Nakaya (University of São Paulo, SP, Brazil) for helping with Bioinformatics Analyses and Dr. Hilde Cheroutre (La Jolla Institute for Immunology, CA, USA) for critically reading our manuscript and enriching discussion.

Funding. This study was financed in part by the Coordenação de Aperfeiçoamento de Pessoal de Nível Superior - Brasil (CAPES) - Finance Code 001; Fundação Carlos Chagas Filho de Amparo à Pesquisa do Estado do Rio de Janeiro (FAPERJ); Conselho Nacional de Pesquisas (CNPq) and by The National Institute for Vaccine Development and Technology (INCTV-CNPq) and National Institutes of Health (NIH). CDB and LMB received PhD fellowships from CNPq; AG and EGAN received PhD fellowships from CAPES; FBC and AG received PDJ-CNPq fellowships. GM received PIBIC-CNPq fellowship. AN, WOD and MB received PQ fellowship from CNPq; AN and MB received CNE grant from FAPERJ.

The funders had no role in study design, data collection and analysis, decision to publish, or preparation of the manuscript.

Author contributions: CDB, FBC, WOD, ACO, AN and MB conceived and designed the experiments. CDB, FBC, AG, LMB, JRL, EGAN, ACO, AN and MB performed the experiments. CDB, FBC, AG, LMB, GAM, ACO, EGAN, WOD, AN and MB analyzed the data. ACO, WOD, AN and MB contributed parasites/reagents/ mice/materials/analysis tools. MB wrote the paper.

842 **Competing interests:** The authors declare no competing financial interests.

843

844 **References:**

845

846 Afonina, I. S., Cullen, S. P., & Martin, S. J. (2010). Cytotoxic and non-cytotoxic roles
847 of the CTL/NK protease granzyme B. *Immunol Rev, 235*(1), 105-116. doi:
848 10.1111/j.0105-2896.2010.00908.x

849 Anderson, A. C., Joller, N., & Kuchroo, V. K. (2016). Lag-3, Tim-3, and TIGIT: Co-
850 inhibitory Receptors with Specialized Functions in Immune Regulation. *Immunity,*
851 *44*(5), 989-1004. doi: 10.1016/j.immuni.2016.05.001

852 Anderson, C. F., Oukka, M., Kuchroo, V. J., & Sacks, D. (2007). CD4(+)CD25(-
853)Foxp3(-) Th1 cells are the source of IL-10-mediated immune suppression in chronic
854 cutaneous leishmaniasis. *J Exp Med., 204*(2), 285-297. Epub 2007
855 doi:10.1084/jem.20061886.

856 Ayo, C. M., Oliveira, A. P., Camargo, A. V., Mattos, C. C., Bestetti, R. B., & Mattos, L.
857 C. (2015). Association of the Functional MICA-129 Polymorphism With the Severity
858 of Chronic Chagas Heart Disease. *Clin Infect Dis, 61*(8), 1310-1313. doi:
859 10.1093/cid/civ540

860 Bannard, O., Kraman, M., & Fearon, D. T. (2009). Secondary replicative function of
861 CD8+ T cells that had developed an effector phenotype. *Science, 323*(5913), 505-509.

862 Baumann, C., Bonilla, W. V., Fröhlich, A., Helmstetter, C., Peine, M., Hegazy, A. N., .
863 . . Löhning, M. (2015). T-bet- and STAT4-dependent IL-33 receptor expression
864 directly promotes antiviral Th1 cell responses. *Proc Natl Acad Sci U S A, 112*(13),
865 4056-4061. doi: 10.1073/pnas.1418549112

866 Bellio, M., Oliveira, A. C., Mermelstein, C. S., Capella, M. A., Viola, J. P., Levraud,

867 J. P., . . . Mendonca-Previato, L. (1999). Costimulatory action of glycoinositol-
868 phospholipids from Trypanosoma cruzi: increased interleukin 2 secretion and
869 induction of nuclear translocation of the nuclear factor of activated T cells 1. *FASEB*
870 *J., 13*(12), 1627-1636. doi: 10.1096/fasebj.13.12.1627.
871 Ben-Sasson, S. Z., Hu-Li, J., Quiel, J., Cauchetaux, S., Ratner, M., Shapira, I., . . . Paul,
872 W. E. (2009). IL-1 acts directly on CD4 T cells to enhance their antigen-driven
873 expansion and differentiation. *Proc Natl Acad Sci U S A, 106*(17), 7119-7124. doi:
874 10.1073/pnas.0902745106.
875 Bern, C. (2015). Chagas' Disease. *New England Journal of Medicine, 373*(5), 456-466.
876 doi: 10.1056/NEJMra1410150
877 Bossi, G., & Griffiths, G. M. (1999). Degranulation plays an essential part in regulating
878 cell surface expression of Fas ligand in T cells and natural killer cells. *Nat Med, 5*(1),
879 90-96. doi: 10.1038/4779
880 Brien, J. D., Uhrlaub, J. L., & Nikolich-Zugich, J. (2008). West Nile virus-specific CD4
881 T cells exhibit direct antiviral cytokine secretion and cytotoxicity and are sufficient
882 for antiviral protection. *J Immunol, 181*(12), 8568-8575. doi:
883 10.4049/jimmunol.181.12.8568.
884 Brown, D. M., Kamperschroer, C., Dilzer, A. M., Roberts, D. M., & Swain, S. L.
885 (2009). IL-2 and antigen dose differentially regulate perforin- and FasL-mediated
886 cytolytic activity in antigen specific CD4+ T cells. *Cell Immunol, 257*(1-2), 69-79.
887 doi: 10.1016/j.cellimm.2009.03.002
888 Brown, D. M., Lee, S., Garcia-Hernandez Mde, L., & Swain, S. L. (2012).
889 Multifunctional CD4 cells expressing gamma interferon and perforin mediate
890 protection against lethal influenza virus infection. *J Virol, 86*(12), 6792-6803. doi:
891 10.1128/jvi.07172-11

892 Burel, J. G., Apte, S. H., Groves, P. L., Klein, K., McCarthy, J. S., & Doolan, D. L.
893 (2016). Reduced Plasmodium Parasite Burden Associates with CD38+ CD4+ T Cells
894 Displaying Cytolytic Potential and Impaired IFN-gamma Production. *PLoS Pathog,*
895 *12*(9), e1005839. doi: 10.1371/journal.ppat.1005839
896 Campos, M. A., Closel, M., Valente, E. P., Cardoso, J. E., Akira, S., Alvarez-Leite, J. I.,
897 . . . Gazzinelli, R. T. (2004). Impaired production of proinflammatory cytokines and
898 host resistance to acute infection with Trypanosoma cruzi in mice lacking functional
899 myeloid differentiation factor 88. *J Immunol, 172*(3), 1711-1718. doi:
900 10.4049/jimmunol.172.3.1711.
901 Canaday, D. H., Wilkinson, R. J., Li, Q., Harding, C. V., Silver, R. F., & Boom, W. H.
902 (2001). CD4(+) and CD8(+) T cells kill intracellular Mycobacterium tuberculosis by a
903 perforin and Fas/Fas ligand-independent mechanism. *J Immunol, 167*(5), 2734-2742.
904 doi: 10.4049/jimmunol.167.5.2734.
905 Cheadle, C., Vawter, M. P., Freed, W. J., & Becker, K. G. (2003). Analysis of
906 microarray data using Z score transformation. *J Mol Diagn, 5*(2), 73-81. doi:
907 10.1016/S1525-1578(10)60455-2.
908 Cheroutre, H., & Husain, M. M. (2013). CD4 CTL: living up to the challenge. *Semin*
909 *Immunol, 25*(4), 273-281. doi: 10.1016/j.smim.2013.10.022.
910 Cooper, D., Pride, M. W., Guo, M., Cutler, M., Mester, J. C., Nasar, F., . . . Natuk, R. J.
911 (2004). Interleukin-12 redirects murine immune responses to soluble or aluminum
912 phosphate adsorbed HSV-2 glycoprotein D towards Th1 and CD4+ CTL responses.
913 *Vaccine, 23*(2), 236-246. doi: 10.1016/j.vaccine.2004.05.011
914 Cordeiro, Z. M., Dahia, A. C., & Andrade, Z. A. (1997). Kinetics of Trypanosoma cruzi
915 destruction in the mouse spleen. *Rev Soc Bras Med Trop, 30*(1), 3-9. doi:
916 10.1590/s0037-86821997000100002

917 Cruz-Guilloty, F., Pipkin, M. E., Djuretic, I. M., Levanon, D., Lotem, J., Lichtenheld,
918 M. G., . . . Rao, A. (2009). Runx3 and T-box proteins cooperate to establish the
919 transcriptional program of effector CTLs. *J Exp Med, 206*(1), 51-59. doi:
920 10.1084/jem.20081242
921 Curran, M. A., Geiger, T. L., Montalvo, W., Kim, M., Reiner, S. L., Al-Shamkhani, A.,
922 . . . Allison, J. P. (2013). Systemic 4-1BB activation induces a novel T cell phenotype
923 driven by high expression of Eomesodermin. *J Exp Med, 210*(4), 743-755. doi:
924 10.1084/jem.20121190
925 Djuretic, I. M., Levanon, D., Negreanu, V., Groner, Y., Rao, A., & Ansel, K. M. (2007).
926 Transcription factors T-bet and Runx3 cooperate to activate Ifng and silence Il4 in T
927 helper type 1 cells. *Nat Immunol, 8*(2), 145-153. doi: 10.1038/ni1424.
928 Donnarumma, T., Young, G. R., Merkenschlager, J., Eksmond, U., Bongard, N., Nutt,
929 S. L., . . . Kassiotis, G. (2016). Opposing Development of Cytotoxic and Follicular
930 Helper CD4 T Cells Controlled by the TCF-1-Bcl6 Nexus. *Cell Rep, 17*(6), 1571-
931 1583. doi: 10.1016/j.celrep.2016.10.013
932 DosReis, G. A., Pecanha, L. M., Bellio, M., Previato, J. O., & Mendonca-Previato, L.
933 (2002). Glycoinositol phospholipids from Trypanosoma cruzi transmit signals to the
934 cells of the host immune system through both ceramide and glycan chains. *Microbes*
935 *Infect., 4*(9), 1007-1013. doi: 10.1016/s1286-4579(02)01616-7.
936 Egawa, T., Tillman, R. E., Naoe, Y., Taniuchi, I., & Littman, D. R. (2007). The role of
937 the Runx transcription factors in thymocyte differentiation and in homeostasis of
938 naive T cells. *J Exp Med, 204*(8), 1945-1957. doi: 10.1084/jem.20070133.
939 Eshima, K., Chiba, S., Suzuki, H., Kokubo, K., Kobayashi, H., Iizuka, M., . . .
940 Shinohara, N. (2012). Ectopic expression of a T-box transcription factor,
941 eomesodermin, renders CD4(+) Th cells cytotoxic by activating both perforin- and

942 FasL-pathways. *Immunol Lett, 144*(1-2), 7-15. doi: 10.1016/j.imlet.2012.02.013
943 Fang, M., Siciliano, N. A., Hersperger, A. R., Roscoe, F., Hu, A., Ma, X., . . . Sigal, L.
944 J. (2012). Perforin-dependent CD4+ T-cell cytotoxicity contributes to control a
945 murine poxvirus infection. *Proc Natl Acad Sci U S A, 109*(25), 9983-9988. doi:
946 10.1073/pnas.1202143109
947 Ferreira, L. R., Frade, A. F., Baron, M. A., Navarro I. C., Kalil, J., Chevillard, C. &
948 Cunha-Neto, E. (2014). Interferon-γ and other inflammatory mediators in
949 cardiomyocyte signaling during Chagas disease cardiomyopathy. *World J Cardiol,*
950 *6*(8), 782-790. doi: 10.4330/wjc.v6.i8.782
951 Ferreira, L. R., Ferreira, F. M., Nakaya, H. I., Deng, X., Cândido, D. D., de Oliveira, L.
952 C., . . . Cunha-Neto, E. (2017). Blood Gene Signatures of Chagas Cardiomyopathy
953 With or Without Ventricular Dysfunction. *J Infect Dis, 215*(3), 387-395. doi:
954 10.1093/infdis/jiw540
955 Frazer, L. C., Sullivan, J. E., Zurenski, M. A., Mintus, M., Tomasak, T. E., Prantner, D.,
956 . . . Darville, T. (2013). CD4+ T cell expression of MyD88 is essential for normal
957 resolution of Chlamydia muridarum genital tract infection. *J Immunol, 191*(8), 4269-
958 4279.
959 Gagliani, N., Magnani, C. F., Huber, S., Gianolini, M. E., Pala, M., Licona-Limon, P., .
960 . . Roncarolo, M. G. (2013). Coexpression of CD49b and LAG-3 identifies human and
961 mouse T regulatory type 1 cells. *Nat Med, 19*(6), 739-746. doi: 10.1038/nm.3179
962 Glimcher, L. H., Townsend, M. J., Sullivan, B. M., & Lord, G. M. (2004). Recent
963 developments in the transcriptional regulation of cytolytic effector cells. *Nat Rev*
964 *Immunol, 4*(11), 900-911. doi: 10.1038/nri1490
965 Gomes-Neto, J. F., Sartorius, R., Canto, F. B., Almeida, T. S., Dias, A. A., Barbosa, C.
966 D., . . . Bellio, M. (2018). Vaccination With Recombinant Filamentous fd Phages

967 Against Parasite Infection Requires TLR9 Expression. *Front Immunol, 9*, 1173. doi:
968 10.3389/fimmu.2018.01173
969 Gunturi, A., Berg, R. E., & Forman, J. (2004). The role of CD94/NKG2 in innate and
970 adaptive immunity. *Immunol Res, 30*(1), 29-34. doi: 10.1385/ir:30:1:029
971 Gutcher, I., Urich, E., Wolter, K., Prinz, M., & Becher, B. (2006). Interleukin 18-
972 independent engagement of interleukin 18 receptor-alpha is required for autoimmune
973 inflammation. *Nat Immunol, 7*(9), 946-953. doi: 10.1038/ni1377.
974 Haring, J. S., & Harty, J. T. (2009). Interleukin-18-related genes are induced during the
975 contraction phase but do not play major roles in regulating the dynamics or function
976 of the T-cell response to Listeria monocytogenes infection. *Infect Immun, 77*(5),
977 1894-1903. doi: 10.1128/IAI.01315-08.
978 Hua, L., Yao, S., Pham, D., Jiang, L., Wright, J., Sawant, D., . . . Sun, J. (2013).
979 Cytokine-dependent induction of CD4+ T cells with cytotoxic potential during
980 influenza virus infection. *J Virol, 87*(21), 11884-11893. doi: 10.1128/jvi.01461-13
981 Hwang, S., Cobb , D. A., Bhadra, R., Youngblood, B. & Khan, I.A. (2016). Blimp-1-
982 mediated CD4 T cell exhaustion causes CD8 T cell dysfunction during chronic
983 toxoplasmosis. *J Exp Med* 213(9):1799-1818. doi: 10.1084/jem.20151995.
984 Intlekofer, A. M., Takemoto, N., Wherry, E. J., Longworth, S. A., Northrup, J. T.,
985 Palanivel, V. R., . . . Reiner, S. L. (2005). Effector and memory CD8+ T cell fate
986 coupled by T-bet and eomesodermin. *Nat Immunol, 6*(12), 1236-1244. doi:
987 10.1038/ni1268
988 Jankovic, D., Kullberg, M. C., Feng, C.G., Goldszmid, R.S., Collazo, C. M., Wilson,
989 M., . . . Sher, A. (2007). Conventional T-bet+FoxP3- Th1 cells are the major source of
990 host-protective regulatory IL-10 during intracellular protozoan infection. *J Exp Med,*
991 *204*(2), 273. doi: 10.1084/jem.20062175

992 Jellison, E. R., Kim, S. K., & Welsh, R. M. (2005). MHC class II-restricted killing in
993 vivo during viral infection. *J Immunol, 174*(2), 614-618. doi:
994 10.4049/jimmunol.174.2.614.
995 Joffre, O., Nolte, M. A., Spörri, R., & Reis e Sousa, C. (2009). Inflammatory signals in
996 dendritic cell activation and the induction of adaptive immunity. *Immunol Rev,*
997 *227*(1), 234-247. doi: 10.1111/j.1600-065X.2008.00718.x
998 Juno, J. A., van Bockel, D., Kent, S. J., Kelleher, A. D., Zaunders, J. J., & Munier, C.
999 M. (2017). Cytotoxic CD4 T Cells-Friend or Foe during Viral Infection? *Front*
1000 *Immunol, 8*, 19. doi: 10.3389/fimmu.2017.00019
1001 Kara, E. E., Comerford, I., Fenix, K. A., Bastow, C. R., Gregor, C. E., McKenzie, D. R.,
1002 & McColl, S. R. (2014). Tailored immune responses: novel effector helper T cell
1003 subsets in protective immunity. *PLoS Pathog, 10*(2), e1003905. doi:
1004 10.1371/journal.ppat.1003905
1005 Keesen, T.S.L., Gomes, J.A.S, Fares, R.C.G., de Araújo, F.F, Ferreira, K.S, Chaves,
1006 A.T, Rocha, M.O.C, Correa-Oliveira, R. (2012). Characterization of CD4+ cytotoxic
1007 lymphocytes and apoptosis markers induced by *Trypanossoma cruzi* infection. *Scand*
1008 *J Immunol,* 76(3), 311-319. doi: 10.1111/j.1365-3083.2012.02730.x.
1009 Kiner, E., Willie, E., Vijaykumar, B., Chowdhary, K., Schmutz, H., Chandler, J., . . .
1010 Benoist, C. (2021). Gut CD4(+) T cell phenotypes are a continuum molded by
1011 microbes, not by T(H) archetypes. *Nat Immunol, 22*(2), 216-228. doi:
1012 10.1038/s41590-020-00836-7
1013 Kotov, D. I., Kotov, J. A., Goldberg, M. F., & Jenkins, M. K. (2018). Many Th Cell
1014 Subsets Have Fas Ligand-Dependent Cytotoxic Potential. *J Immunol, 200*(6), 2004-
1015 2012. doi: 10.4049/jimmunol.1700420
1016 Krueger, P. D., Goldberg, M. F., Hong, S. W., Osum, K. C., Langlois, R. A., Kotov,

1017 D. I., . . . Jenkins, M. K. (2021). Two sequential activation modules control the
1018 differentiation of protective T helper-1 (Th1) cells. *Immunity, 54*(4), 687-701 e684.
1019 doi: 10.1016/j.immuni.2021.03.006
1020 LaRosa, D. F., Stumhofer, J. S., Gelman, A. E., Rahman, A. H., Taylor, D. K., Hunter,
1021 C. A., & Turka, L. A. (2008). T cell expression of MyD88 is required for resistance to
1022 Toxoplasma gondii. *Proc Natl Acad Sci U S A, 105*(10), 3855-3860. doi:
1023 10.1073/pnas.0706663105.
1024 Leon Rodriguez, D.A., Carmona, F. D., Echeverría, L. E., González, C. I., & Martin, J.
1025 (2016). IL18 Gene Variants Influence the Susceptibility to Chagas Disease. *PLOS*
1026 *Negl Trop Dis, 10*(3), e0004583. doi: 10.1371/journal.pntd.0004583
1027 Lewis, E. C., & Dinarello, C. A. (2006). Responses of IL-18- and IL-18 receptor-
1028 deficient pancreatic islets with convergence of positive and negative signals for the
1029 IL-18 receptor. *Proc Natl Acad Sci U S A, 103*(45), 16852-16857. doi:
1030 10.1073/pnas.0607917103.
1031 Machado F.S., Martins, G. A., Aliberti, J. C. , Mestriner, F. L., Cunha, F. Q. & Silva
1032 J.S. (2000). *Trypanosoma cruzi*-infected cardiomyocytes produce chemokines and
1033 cytokines that trigger potent nitric oxide-dependent trypanocidal activity. *Circulation*
1034 *102*(24):3003-3008. doi: 10.1161/01.cir.102.24.3003
1035 Marshall, N. B., Vong, A. M., Devarajan, P., Brauner, M. D., Kuang, Y., Nayar, R., . . .
1036 Swain, S. L. (2017). NKG2C/E Marks the Unique Cytotoxic CD4 T Cell Subset,
1037 ThCTL, Generated by Influenza Infection. *J Immunol, 198*(3), 1142-1155. doi:
1038 10.4049/jimmunol.1601297
1039 Mascanfroni, I. D., Takenaka, M. C., Yeste, A., Patel, B., Wu, Y., Kenison, J. E., . . .
1040 Quintana, F. J. (2015). Metabolic control of type 1 regulatory T cell differentiation by
1041 AHR and HIF1-alpha. *Nat Med, 21*(6), 638-646. doi: 10.1038/nm.3868

1042 Medeiros, M. M., Peixoto, J. R., Oliveira, A. C., Cardilo-Reis, L., Koatz, V. L., Van
1043 Kaer, L., . . . Bellio, M. (2007). Toll-like receptor 4 (TLR4)-dependent
1044 proinflammatory and immunomodulatory properties of the glycoinositolphospholipid
1045 (GIPL) from *Trypanosoma cruzi. J Leukoc Biol, 82*(3), 488-496. doi:
1046 10.1189/jlb.0706478.
1047 Menezes, C. A., Sullivan, A. K., Falta, M. T., Mack, D. G., Freed, B. M., Rocha, M. O.,
1048 . . . Dutra, W. O. (2012). Highly conserved CDR3 region in circulating
1049 CD4(+)Vbeta5(+) T cells may be associated with cytotoxic activity in Chagas disease.
1050 *Clin Exp Immunol, 169*(2), 109-118. doi: 10.1111/j.1365-2249.2012.04608.x.
1051 Millar, A. E., & Kahn, S. J. (2000). The SA85-1.1 protein of the Trypanosoma cruzi
1052 trans-sialidase superfamily is a dominant T-cell antigen. *Infect Immun, 68*(6), 3574-
1053 3580. doi: 10.1128/IAI.68.6.3574-3580.2000.
1054 Mittal, P., Abblett, R., Ryan, J. M., Hagymasi, A. T., Agyekum-Yamoah, A., Svedova,
1055 J., . . . Adler, A. J. (2018). An Immunotherapeutic CD137 Agonist Releases
1056 Eomesodermin from ThPOK Repression in CD4 T Cells. *J Immunol, 200*(4), 1513-
1057 1526. doi: 10.4049/jimmunol.1701039
1058 Monteforte, G. M., Takeda, K., Rodriguez-Sosa, M., Akira, S., David, J. R., & Satoskar,
1059 A. R. (2000). Genetically Resistant Mice Lacking IL-18 Gene Develop Th1 Response
1060 and Control Cutaneous *Leishmania major* Infection. *J Immunol 164*(11), 5890-5893.
1061 doi: 10.4049/jimmunol.164.11.5890
1062 Mucida, D., Husain, M. M., Muroi, S., van Wijk, F., Shinnakasu, R., Naoe, Y., . . .
1063 Cheroutre, H. (2013). Transcriptional reprogramming of mature CD4(+) helper T
1064 cells generates distinct MHC class II-restricted cytotoxic T lymphocytes. *Nat*
1065 *Immunol, 14*(3), 281-289. doi: 10.1038/ni.2523.
1066 Nakahira, M., Tomura, M., Iwasaki, M., Ahn, H., Bian, Y., Hamaoka, T., . . .

1067 Fujiwara, H. (2001). An Absolute Requirement for STAT4 and a Role for IFN-γ as an
1068 Amplifying Factor in IL-12 Induction of the Functional IL-18 Receptor Complex. *J*
1069 *Immunol, 167*(3), 1306. doi: 10.4049/jimmunol.167.3.1306
1070 Nogueira, L. G., Frade, A. F., Ianni, B. M., Laugier, L., Pissetti, C. W., Cabantous, S., .
1071 . . Cunha-Neto, E. (2015). Functional IL18 polymorphism and susceptibility to
1072 Chronic Chagas Disease. *Cytokine, 73*(1), 79-83. doi:
1073 https://doi.org/10.1016/j.cyto.2015.01.037
1074 Nunes, M. C. P., Beaton, A., Acquatella, H., Bern, C., Bolger, A. F., Echeverría, L. E., .
1075 . . Marin-Neto, J. A. (2018). Chagas Cardiomyopathy: An Update of Current Clinical
1076 Knowledge and Management: A Scientific Statement From the American Heart
1077 Association. *Circulation, 138*(12), e169-e209. doi: 10.1161/cir.0000000000000599
1078 Oliveira, A. C., de Alencar, B. C., Tzelepis, F., Klezewsky, W., da Silva, R. N., Neves,
1079 F. S., . . . Bellio, M. (2010). Impaired innate immunity in Tlr4(-/-) mice but preserved
1080 CD8+ T cell responses against *Trypanosoma cruzi* in Tlr4-, Tlr2-, Tlr9- or Myd88-
1081 deficient mice. *PLoS Pathog, 6*(4), e1000870. doi: 10.1371/journal.ppat.1000870
1082 Oliveira, A. C., Gomes-Neto, J. F., Barbosa, C. D., Granato, A., Reis, B. S., Santos, B.
1083 M., . . . Bellio, M. (2017). Crucial role for T cell-intrinsic IL-18R-MyD88 signaling in
1084 cognate immune response to intracellular parasite infection. *Elife, 6*. doi:
1085 10.7554/eLife.30883
1086 Park, Y., Ryu, H., Choi, G., Kim, B., Hwang, E. S., Kim, H. S., & Chung, Y. (2019).
1087 IL-27 confers a protumorigenic activity of regulatory T cells via CD39. *Proc Natl*
1088 *Acad Sci U S A,* 116(8):3106-3111. doi: 10.1073/pnas.1810254116
1089 Pearce, E. L., Mullen, A. C., Martins, G. A., Krawczyk, C.M., Hutchins, A. S., Zediak,
1090 V. P., . . . Reiner, S. L. (2003). Control of Effector CD8+ T Cell Function by the
1091 Transcription Factor Eomesodermin. *Science, 302*(5647), 1041-1043. doi:

10.1126/science.1090148

Poholek, A. C. (2021). Tissue-Specific Contributions to Control of T Cell Immunity. *Immunohorizons, 5*(6), 410-423. doi: 10.4049/immunohorizons.2000103

Quezada, S. A., Simpson T.R., Peggs K.S., Merghoub T., Vider J., Fan X., … Allison J.P. (2010). Tumor-reactive CD4(+) T cells develop cytotoxic activity and eradicate large established melanoma after transfer into lymphopenic hosts. *J Exp Med* 207 (3), 637–650. doi: 10.1084/jem.20091918

Qui, H. Z., Hagymasi, A. T., Bandyopadhyay, S., St Rose, M. C., Ramanarasimhaiah, R., Menoret, A., . . . Adler, A. J. (2011). CD134 plus CD137 dual costimulation induces Eomesodermin in CD4 T cells to program cytotoxic Th1 differentiation. *J Immunol, 187*(7), 3555-3564. doi: 10.4049/jimmunol.1101244

Reis, B. S., Rogoz, A., Costa-Pinto, F. A., Taniuchi, I., & Mucida, D. (2013). Mutual expression of the transcription factors Runx3 and ThPOK regulates intestinal CD4(+) T cell immunity. *Nat Immunol, 14*(3), 271-280. doi: 10.1038/ni.2518.

Reis, D. D., Jones, E. M., Tostes, S., Lopes, E. R., Chapadeiro, E., Gazzinelli, G., . . . McCurley, T. L. (1993). Expression of major histocompatibility complex antigens and adhesion molecules in hearts of patients with chronic Chagas' disease. *Am J Trop Med Hyg, 49*(2), 192-200. doi: 10.4269/ajtmh.1993.49.192.

Robinson, D., Shibuya, K., Mui, A., Zonin, F., Murphy, E., Sana, T., . . . O'Garra, A. (1997). IGIF does not drive Th1 development but synergizes with IL-12 for interferon-gamma production and activates IRAK and NFkappaB. *Immunity, 7*(4), 571-581. doi: 10.1016/s1074-7613(00)80378-7

Rodrigues, M. M., Oliveira, A. C., & Bellio, M. (2012). The Immune Response to Trypanosoma cruzi: Role of Toll-Like Receptors and Perspectives for Vaccine Development. *J Parasitol Res, 2012*, 507874. doi: 10.1155/2012/507874

1117 Roncarolo, M. G., Gregori, S., Bacchetta, R., Battaglia, M., & Gagliani, N. (2018). The
1118 Biology of T Regulatory Type 1 Cells and Their Therapeutic Application in Immune-
1119 Mediated Diseases. *Immunity, 49*(6), 1004-1019. doi: 10.1016/j.immuni.2018.12.001
1120 Schenten, D., Nish, S. A., Yu, S., Yan, X., Lee, H. K., Brodsky, I., . . . Medzhitov, R.
1121 (2014). Signaling through the Adaptor Molecule MyD88 in CD4+ T Cells Is Required
1122 to Overcome Suppression by Regulatory T Cells. *Immunity, 40*(1), 78-90. doi:
1123 10.1016/j.immuni.2013.10.023.
1124 Serroukh, Y., Gu-Trantien, C., Kashani, B.H., Defrance, M., Vu Manh, T. P., Azouz,
1125 A., . . . Marchant, A. (2018). The transcription factors Runx3 and ThPOK cross-
1126 regulate acquisition of cytotoxic function by human Th1 lymphocytes. *Elife, 7*. doi:
1127 10.7554/eLife.30496
1128 Smeltz, R. B., Chen, J., Hu-Li, J., & Shevach, E. M. (2001). Regulation of interleukin
1129 (IL)-18 receptor alpha chain expression on CD4(+) T cells during T helper (Th)1/Th2
1130 differentiation. Critical downregulatory role of IL-4. *J Exp Med, 194*(2), 143-153. doi:
1131 10.1084/jem.194.2.143
1132 Stojanovic, A., Correia, M. P., & Cerwenka, A. (2018). The NKG2D/NKG2DL Axis in
1133 the Crosstalk Between Lymphoid and Myeloid Cells in Health and Disease. *Front*
1134 *Immunol, 9*, 827. doi: 10.3389/fimmu.2018.00827
1135 Tagawa, T., Albanese, M., Bouvet, M., Moosmann, A., Mautner, J., Heissmeyer, V., . . .
1136 Hammerschmidt, W. (2016). Epstein-Barr viral miRNAs inhibit antiviral CD4+ T cell
1137 responses targeting IL-12 and peptide processing. *J Exp Med, 213*(10), 2065-2080.
1138 doi: 10.1084/jem.20160248
1139 Takeda, K., Tsutsui, H., Yoshimoto, T., Adachi, O., Yoshida, N., Kishimoto, T., . . .
1140 Akira, S. (1998). Defective NK cell activity and Th1 response in IL-18-deficient
1141 mice. *Immunity, 8*(3), 383-390. doi: 10.1016/s1074-7613(00)80543-9.

1142 Takeuchi, A., Badr Mel, S., Miyauchi, K., Ishihara, C., Onishi, R., Guo, Z., . . . Saito, T.
1143 (2016). CRTAM determines the CD4+ cytotoxic T lymphocyte lineage. *J Exp Med,*
1144 *213*(1), 123-138. doi: 10.1084/jem.20150519
1145 Takeuchi, A., & Saito, T. (2017). CD4 CTL, a Cytotoxic Subset of CD4(+) T Cells,
1146 Their Differentiation and Function. *Front Immunol, 8*, 194. doi:
1147 10.3389/fimmu.2017.00194
1148 Wensveen, F. M., Jelencic, V., & Polic, B. (2018). NKG2D: A Master Regulator of
1149 Immune Cell Responsiveness. *Front Immunol, 9*, 441. doi:
1150 10.3389/fimmu.2018.00441
1151 Wherry, E.J. (2011) T cell exhaustion. *Nature Immunol 12*(6), 492-499.
1152 doi:10.1038/ni.2035
1153 Wilkinson, T. M., Li, C. K., Chui, C. S., Huang, A. K., Perkins, M., Liebner, J. C., . . .
1154 Xu, X. N. (2012). Preexisting influenza-specific CD4+ T cells correlate with disease
1155 protection against influenza challenge in humans. *Nat Med, 18*(2), 274-280. doi:
1156 10.1038/nm.2612
1157 Xie, Y., Akpinarli, A., Maris, C., Hipkiss, E. L., Lane, M., Kwon, E. K., . . . Antony, P.
1158 A. (2010). Naive tumor-specific CD4(+) T cells differentiated in vivo eradicate
1159 established melanoma. *J Exp Med, 207*(3), 651-667. doi: 10.1084/jem.20091921
1160 Zhang, P., Lee, J. S., Gartlan, K.H., Schuster, I.S., Comerford, I., Varelias, A., . . . Hill,
1161 G. R. (2017). Eomesodermin promotes the development of type 1 regulatory T (T_{R1})
1162 cells. *Sci Immunol, 2*(10), eaah7152. doi: 10.1126/sciimmunol.aah7152

1163 **Figure Legends:**

1164 **Figure 1: $CD4^+GzB^+PRF^+$ T cells are present at high frequency in the spleen of**
1165 **mice infected with *T. cruzi.* (A)** $CD4^+$ T cell gating strategy **(B and C)** Representative
1166 flow-cytometry dot plots of GzB **(B)** or PRF **(C)** staining, gated on $CD4^+$ T cells from
1167 non-infected or infected B6 mice (left) and mean frequency of $CD4^+GzB^+$ (or
1168 $CD4^+PRF^+$) T cells in the spleen (right). **(D)** Representative dot plots of PRF and GzB
1169 expression in $CD4^+$ T cells gated as in (A) and mean frequencies of PFR^+ among GzB^+
1170 $CD4^+$ T cells (isotype controls on Figure 1-figure supplement 1A). **(E)** Representative
1171 histogram of 2B4 (CD244) expression on $CD8^+$ (blue), $CD4^+GzB^+$ (red) or $CD4^+GzB^-$
1172 T cells (pink), and correspondent mean MFI values; **(F)** Representative dot plots of
1173 GzB and IFN-γ staining in gated $CD4^+$ T splenocytes (left), mean frequencies of
1174 $GzB^+IFN\text{-}\gamma^-$ (red), $GzB^+IFN\text{-}\gamma^+$ (purple) and $GzB^-IFN\text{-}\gamma^+$ (blue) subsets among
1175 total $CD4^+$ (center) or gated on $CD4^+GzB^+$ T cells (right). (**G)** Kinetics of the mean
1176 frequency of $CD4^+IFN\text{-}\gamma^+$ (purple) and $CD4^+GzB^+$ (red) (left), and corresponding
1177 absolute numbers (right). **(H)** Frequency of LAMP-1^+($CD107a^+$) cells among
1178 $CD4^+GzB^+$ (red) or $CD8^+GzB^+$ (blue) T cells in the infected spleen. Data obtained from
1179 individually analyzed mice (n=4), at indicated or 14 day pi. Error bars= SEM. ND=
1180 non-detected. *ns*= non-significant; **= $p \leq 0.01$ (Student t test). Data are representative
1181 of 3 or more independent experiments.

1182

1183 **Figure 2: CD4 T cell-mediated Ag-specific cytotoxicity and TF expression by**
1184 **$CD4^+GzB^+$ T cells. (A)** Mean frequencies of dead target cells (LPS-induced B blasts) in
1185 redirected cytotoxicity assay employing sorted naïve (blue) or *in vivo* activated (red)
1186 $CD4^+$ T cells as effectors, at different E:T ratios, in triplicates. **(B)** Specific lysis of IC-
1187 21 macrophages (T) loaded with amastigote antigens, co-incubated with highly

1188 purified effector $CD4^+$ T cells (E), at the indicated E:T ratios, in the presence of anti-
1189 FasL mAb (red) or isotype control mAb (blue). Mean values of triplicates ± SEM are
1190 shown in **(A)** and **(B)**; *$p \leq 0.05$ (two-tailed Student t-test). Data are representative of 3
1191 independent experiments. Gating strategy on Figure 2-figure supplement 1A. (**C and D)**
1192 Percentages of Ag-specific cytotoxicity *in vivo*; bars represent mean values + SEM
1193 (error bars) of individually analyzed mice (n=3) infected with *T. cruzi* Y in **(C)** or Y-
1194 OVA strain in **(D)**; class I-restricted (PA8 or $OVA_{257-264}$) and class II-restricted
1195 (SA851.1c+d or $OVA_{323-339}$) peptides were employed. Data are representative of 2
1196 independent experiments. Cell survival was measured by flow cytometry (Figure 2-
1197 figure supplement 1B) and specific lysis calculated as described in Methods. (**E and F)**
1198 Representative dot plots of $CD4^+$ T cells (gated as in Figure 1A) and corresponding
1199 mean frequencies of gated subpopulations: **(E)** GzB and FoxP3 staining and **(F)** GzB
1200 and T-bet staining. **(G)** Representative histogram of Eomes expression in $CD4^+$ T
1201 splenocytes of non-infected mice (ctr, gray) and in GzB^- (black) and GzB^+ (red) $CD4^+$ T
1202 cells from infected mice, gated as in Figs. 1A and 1B (left) and mean frequencies of
1203 $Eomes^+$ cells among these different subpopulations (right). All experiments were done
1204 at day 14 pi. Bars represent mean values of non-infected ctr group n=3 or infected
1205 group, n=3 to 5, individually analyzed mice. Error bars= SEM. **(H)** Runx3d and ThPOK
1206 (*Zbtb7b*) mRNA expression estimated by qRT-PCR in $CD4^+EYFP^+$ T cells sorted from
1207 infected and tamoxifen-treated $GzmbCreER^{T2}$/ROSA26EYFP mice, as described in
1208 Methods and shown in Figure 2-figure supplement 3A; ND = not detected. Data are
1209 representative of 3 independent experiments.
1210
1211 **Figure 3: Expression of IL-10, immunoregulatory molecules and cytotoxic**
1212 **markers by $CD4^+GzB^+$ T cells. (A)** Representative dot plots of IL-10 staining and

1213 mean frequencies of IL-10$^+$ cells among non-infected (ctr, gray) or GzB$^-$ (black) and
1214 GzB$^+$ (red) CD4$^+$ T cells from infected mice. **(B)** Representative histogram of Lag-3
1215 staining and mean frequency of Lag-3$^+$ cells. **(C)** Representative dot plots of Lag-3 and
1216 CD49b staining and mean frequency of different cells subsets. **(D)** Representative
1217 histogram of Tim-3 staining and mean frequency of Tim-3$^+$ cells among different cells
1218 subsets. **(E)** Representative histogram of CD27 staining and mean frequency of CD27$^+$
1219 cells. **(A-E)** CD4$^+$GzB$^+$ T cells gated as in Figures 1A-1B; staining controls in Figure 3-
1220 figure supplement 1. **(F-H)** Representative dot plots and mean frequencies of **(F)**
1221 NKG2A/C/E, **(G)** NKG2D and **(H)** CRTAM expression among gated CD4$^+$ T
1222 splenocytes. All experiments were done at day 14 pi. Non-infected ctr group, n=3;
1223 infected group, n=3 to 5 mice, individually analyzed. Error bars= SEM; *p≤ 0.05;
1224 ***p≤ 0.001; ****p≤ 0.0001 (two-tailed Student t-test). Data are representative of 3
1225 independent experiments. Staining controls are shown on Figure 3-figure supplement 2.
1226

1227 **Figure 4: CD4CTLs are severely reduced in *Myd88*$^{-/-}$ mice. (A-B)** Representative dot
1228 plots of GzB and T-bet staining on gated CD4$^+$ T splenocytes (left panels) and mean
1229 frequencies of T-bet$^+$, IFN-γ$^+$ and GzB$^+$ CD4$^+$ T cells and absolute numbers of
1230 GzB$^+$CD4$^+$ T cells (on the right) from **(A)** WT (B6) and *Il12p40*$^{-/-}$ mice on day 14 pi
1231 and **(B)** WT and *Ifng*$^{-/-}$ mice on day 11 pi. **(C)** Representative dot plots and gating
1232 strategy. **(D)** Mean frequencies and **(E)** absolute numbers of GzB$^+$ or NKG2A/C/E$^+$,
1233 NKG2D$^+$ and CRTAM$^+$ cells among GzB$^+$CD4$^+$ T cells in the spleen of WT (blue) and
1234 *Myd88*$^{-/-}$ (red) mice at day 13 pi. Bars represent mean values in each group; n= 5
1235 individually analyzed mice. Error bars= SEM; ns= non-significant; *p≤ 0.05; **p≤
1236 0.01; ****p≤ 0.0001 (Student t-test). Representative dot plots of GzB, NKG2A/C/E,
1237 NKG2D and CRTAM staining on CD4$^+$ T cells from non-infected animals are shown

1238 in Figure 4-figure supplement 1B. **(F-G)** Frequencies (left) and absolute numbers
1239 (right) of PRF^+ cells among $CD4^+$ T cells **(F)** and of PRF^+ cells among GzB^+CD4^+ T
1240 cells **(G)** in the spleen of WT (blue bars) and *Myd88*$^{-/-}$ (red bars) mice. GzB^+CD4^+ T
1241 cells were gated as shown in Figs. 1A, 1B and 1G. Data in **(F)** and **(G)** are compiled
1242 from four independent experiments with n= 3 animals in each group, each symbol
1243 represents an individual analyzed mice. **(H)** Frequency of dead target cells (LPS-
1244 induced B cell blasts) in cytotoxic assay, after 14 h of co-culture with $CD4^+CD44^{hi}$ T
1245 cells sorted from WT (blue line) or *Myd88*$^{-/-}$ (red line) infected mice at day 13 pi. B cells
1246 were coated with anti-CD3 (left) or not (right). Mean of triplicates +/- SEM for each
1247 E:T ratio point are shown. Data are representative of 3 independent experiments.
1248

1249 **Figure 5: The CD4CTL gene program is absent in MyD88-deficient $CD4^+$ T cells.**
1250 **(A)** GSEA performed using pre-ranked list of genes expressed in WT or *Myd88*$^{-/-}$ $CD4^+$
1251 T cells sorted from mix-BM chimeras using the CD4CTL gene signature previously
1252 described as gene set (66). **(B)** Venn diagram of CD4CTL genes upregulated in WT and
1253 downregulated in *Myd88*$^{-/-}$ $CD4^+$ T cells sorted from chimeric mice. **(C)** Heat map of
1254 normalized CD4CTL-signature gene expression in WT or *Myd88*$^{-/-}$ $CD4^+$ T cells sorted
1255 from chimeric mice: values indicate mean Z-score, upregulated genes in red and
1256 downregulated genes in blue. **(D)** Representative histograms of Blimp-1 expression
1257 (right) and mean frequency of Blimp-1^+ splenocytes (left) among total gated $CD4^+$ T
1258 cells from non-infected mice (ctr, gray shaded area and bar) or among $CD4^+GzB^+$ (red
1259 line and bar) or $CD4^+GzB^-$ (black line and bar) from WT infected mice at day 14 pi.
1260 Individually analyzed mice, n=4. Error bars=SEM, data are representative of 2
1261 independent experiments. **(E)** Representative histograms (left and central panel) and
1262 mean MFI values of CD39 expression (right panel) on gated $FoxP3^-$ (gray shaded area

1263 and bar) or FoxP3^{+} (blue line and bar) CD4^{+} T cells from non-infected (ctr) mice (left);
1264 GzB^{-}FoxP3^{-} (black line and bar), GzB^{-}FoxP3^{+} (purple line and bar) or GzB^{+}FoxP3^{-} (red
1265 line and bar) CD4^{+} T cells from infected WT mice (center), at day 14 pi; individually
1266 analyzed mice (n=4), error bars =SEM; data are representative of 4 independent
1267 experiments. **(F)** Mean frequency (left) and absolute numbers (right) of GzB-expressing
1268 cells among CD45.1^{+} (B6.SJL WT) or CD45.2^{+} (B6 WT or KO) CD4^{+} T splenocytes in
1269 mix-BM chimeric mice, at day 14 pi; WT:WT control chimera group, n=3; other
1270 chimera groups, n=6 or 7. Error bars= SEM, *ns*= non-significant, ***p≤ 0.001,****p≤
1271 0.0001 (Student t-test). Gating strategy and representative dot plots are shown in Figure
1272 5-figure supplement 1. Data are representative of 3 independent experiments.
1273
1274 **Figure 6: CD4CTLs are severely reduced in *Il18ra*$^{-/-}$ mice. (A and B)** Frequencies
1275 and absolute numbers of PRF^{+} cells among CD4^{+} T cells **(A)** and of PRF^{+} cells among
1276 GzB^{+}CD4^{+} T cells **(B)** in WT (blue bars) and *Il18ra*$^{-/-}$ (red bars) spleens. Data are
1277 compiled from two independent experiments with n= 4-5 animals in each group, each
1278 symbol represents an individual mouse. **(C)** Representative dot plots of GzB, CRTAM,
1279 NKG2D and NKG2A/C/E staining in WT and *Il18ra*$^{-/-}$ mice. **(D)** Mean frequencies and
1280 **(E)** absolute numbers of GzB^{+} or CRTAM^{+}, NKG2D^{+} and NKG2A/C/E^{+} cells among
1281 CD4^{+} and CD4^{+}GzB^{+} T cells, respectively. **(A-E)** CD4^{+} T cells gated as in Figs. 1A-1D;
1282 n=4 individually analyzed mice in each group; error bars= SEM, *p≤ 0.05, **p≤ 0.01,
1283 ***p≤ 0.001, *ns*= non-significant (Student t-test). Data are representative of 2
1284 independent experiments. **(F)** Frequency of dead target cells (LPS-induced B cell blasts)
1285 in cytotoxic assay, after 14 h of co-culture with CD4^{+}CD44^{hi} T cells sorted from WT
1286 (blue line) or *Il18ra*$^{-/-}$ (red line) infected mice at day 13 pi. B cells were coated with
1287 anti-CD3 (left) or not (right). Mean of triplicates +/- SEM for each E:T ratio point are

1288 shown. **(G)** Survival curve (left) and parasite load in the heart (right) of infected *Il18ra*$^{-}$
1289 $^{/-}$ mice, adoptively transferred with CD4^{+}GzBYFP^{+} cells at day 7 pi (red curve and bar),
1290 or not (black curve and bar); time-line in Figure 6-figure supplement 1; n=10 mice in
1291 each group; p = 0.0277; survival data are compiled from two independent experiments.
1292
1293 **Figure 7: Cells with CD4CTL phenotype predominate in the cardiac tissue of**
1294 **infected mice and are at higher frequencies in patients with Chagas**
1295 **cardiomyopathy. (A)** Representative dot plots (gated as in Figure 7-figure supplement
1296 1A), and mean frequency of CD8^{+} and CD4^{+} T cells infiltrating the heart of B6 infected
1297 mice at day 14 pi. **(B and C)** Representative dot plot and mean frequency of **(B)** GzB^{+}
1298 and **(C)** LAMP-1^{+} (CD107a^{+}) cells, among gated CD4^{+} T cells infiltrating the infected
1299 heart; ctr= non-infected, ND= non-detected. **(D)** Mean parasite load in the cardiac tissue
1300 at different time points pi, obtained by real-time PCR, of individually analyzed mice as
1301 described in Methods; Data are representative of at least 8 **(A and B)** or 2 **(C and D)**
1302 independent experiments. **(E)** Representative dot plots and mean frequency of
1303 CRTAM^{+} and NKG2D^{+} cells among gated intracardiac CD4^{+}GzB^{+} T cells. DP=
1304 CRTAM^{+} NKG2D^{+} double positive cells. Individually analyzed mice, n= 4; error bars=
1305 SEM; data are representative of 4 independent experiments. **(F)** Representative dot plots
1306 and mean frequency of PRF^{+} and GzB^{+}PRF^{+} cells among intracardiac CD4^{+}GzB^{+} T
1307 cells; data are compiled from two independent experiments with n= 4 or 5 animals in
1308 each group, each symbol represents an individual analyzed mice. **(G)** Intensity of PRF
1309 staining (MFI) and **(H)** Frequency of PRF^{+} cells among CD4^{+} T cells in PBMCs from
1310 patients with chronic Chagas disease cardiomyopathy (CC; n=10) and healthy donors
1311 (HD; n=4) cultured overnight in medium alone (ctr) or in the presence of
1312 trypomastigote antigens (+trypo); *p≤ 0.05, **p≤ 0.01, *ns*= non-significant; data

1313 analyzed by paired Student t test. **(I)** Frequency of PRF^+ cells among $CD4^+$ T cells in
1314 the peripheral blood of patients with chronic Chagas disease cardiomyopathy (CC;
1315 n=10) and healthy donors (HD; n=4) cultured ON in the presence of trypomastigote
1316 antigens. Gating strategy and representative dot plots are shown in Figure 7-figure
1317 supplement 5. **(J)** Correlation analysis between the percentage of $CD4^+PRF^+$ T cells
1318 among $CD4^+$ T cells in PBMCs from CC patients and left ventricular ejection fraction
1319 (LVEF) (left panel) or left atrium diameter (right panel); indicated *p* and *r* values were
1320 calculated using Pearson correlation test.

Figure 1

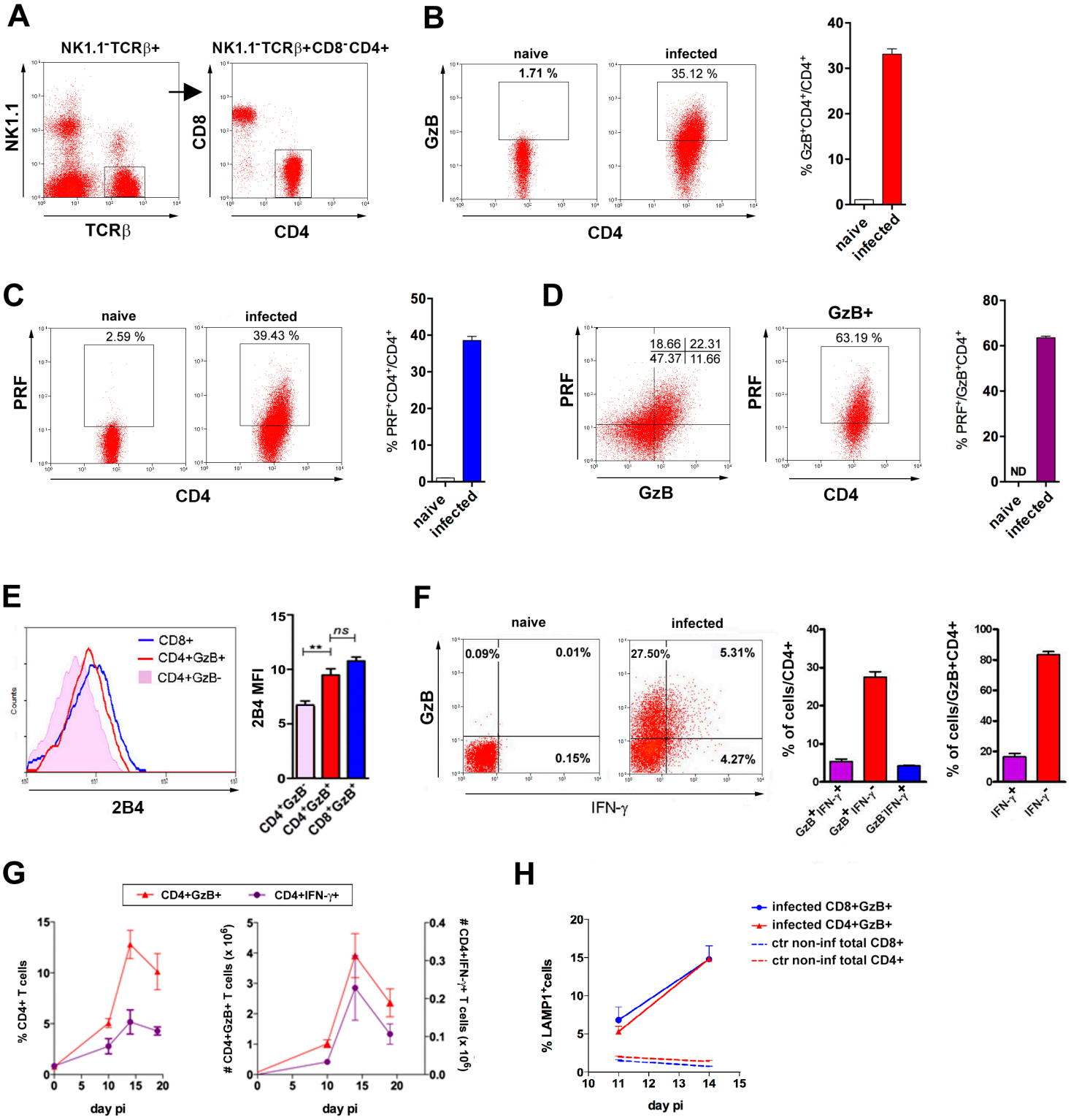
A
NK1.1⁻TCRβ+
NK1.1⁻TCRβ+CD8⁻CD4+
NK1.1
TCRβ
CD8
CD4
B
naive
infected
1.71 %
35.12 %
GzB
CD4
% GzB⁺CD4⁺/CD4⁺
naive
infected
C
naive
infected
2.59 %
39.43 %
PRF
CD4
% PRF⁺CD4⁺/CD4⁺
naive
infected
D
18.66
22.31
47.37
11.66
PRF
GzB
GzB+
63.19 %
PRF
CD4
% PRF⁺/GzB⁺CD4⁺
ND
naive
infected
E
CD8+
CD4+GzB+
CD4+GzB-
Counts
2B4
2B4 MFI
**
ns
CD4⁺GzB⁻
CD4⁺GzB⁺
CD8⁺GzB⁺
F
naive
infected
0.09%
0.01%
0.15%
27.50%
5.31%
4.27%
GzB
IFN-γ
% of cells/CD4+
GzB⁺IFN-γ⁺
GzB⁺IFN-γ⁻
GzB⁻IFN-γ⁺
% of cells/GzB+CD4+
IFN-γ⁺
IFN-γ⁻
G
CD4+GzB+
CD4+IFN-γ+
% CD4+ T cells
day pi
CD4+GzB+ T cells (x 10⁶)
CD4+IFN-γ+ T cells (x 10⁶)
day pi
H
infected CD8+GzB+
infected CD4+GzB+
ctr non-inf total CD8+
ctr non-inf total CD4+
% LAMP1⁺cells
day pi

Figure 2

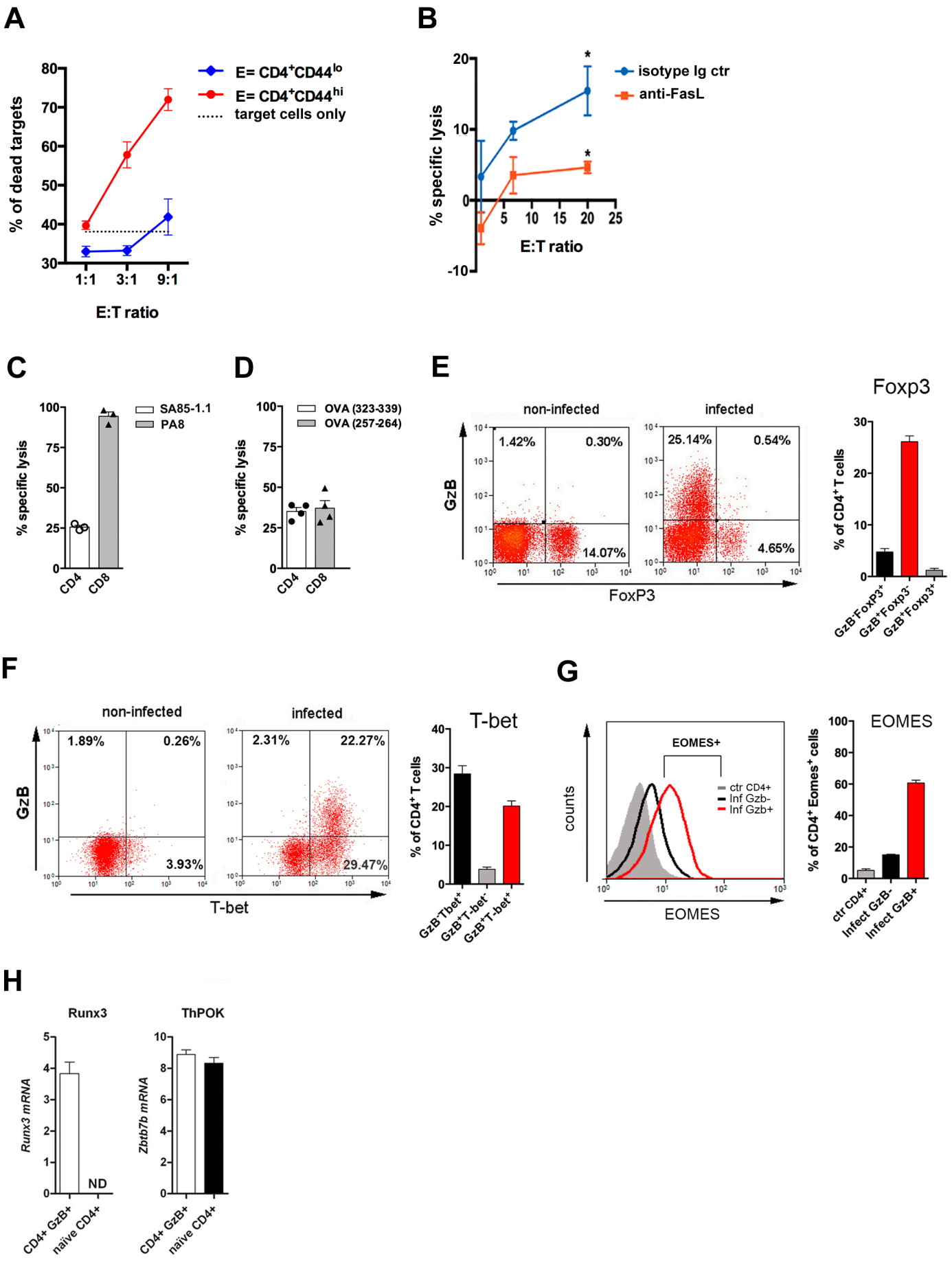
A
% of dead targets
E:T ratio
1:1
3:1
9:1
E= CD4+CD44lo
E= CD4+CD44hi
target cells only
B
% specific lysis
E:T ratio
isotype Ig ctr
anti-FasL
C
% specific lysis
SA85-1.1
PA8
CD4
CD8
D
% specific lysis
OVA (323-339)
OVA (257-264)
CD4
CD8
E
non-infected
infected
GzB
FoxP3
1.42%
0.30%
14.07%
25.14%
0.54%
4.65%
Foxp3
% of CD4+ T cells
GzB-FoxP3+
GzB+Foxp3-
GzB+Foxp3+
F
non-infected
infected
GzB
T-bet
1.89%
0.26%
3.93%
2.31%
22.27%
29.47%
T-bet
% of CD4+ T cells
GzB-Tbet+
GzB+T-bet-
GzB+T-bet+
G
counts
EOMES
EOMES+
ctr CD4+
Inf Gzb-
Inf Gzb+
EOMES
% of CD4+ Eomes+ cells
ctr CD4+
Infect GzB-
Infect GzB+
H
Runx3
ThPOK
Runx3 mRNA
Zbtb7b mRNA
ND
CD4+ GzB+
naïve CD4+
CD4+ GzB+
naïve CD4+

Figure 3

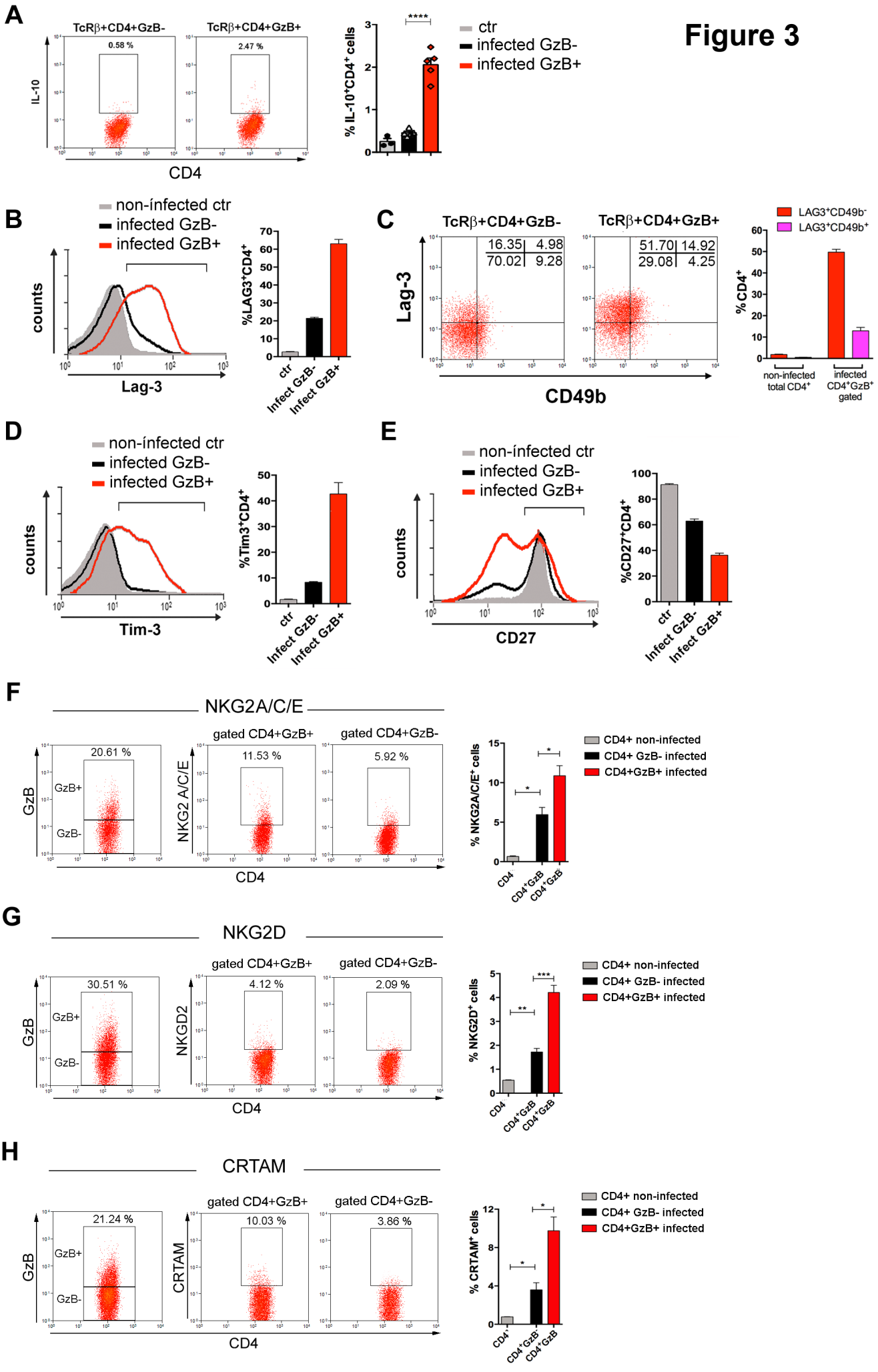
A
TcRβ+CD4+GzB-
TcRβ+CD4+GzB+
0.58 %
2.47 %
IL-10
CD4
% IL-10+CD4+ cells
****
ctr
infected GzB-
infected GzB+
B
non-infected ctr
infected GzB-
infected GzB+
counts
Lag-3
%LAG3+CD4+
ctr
Infect GzB-
Infect GzB+
C
TcRβ+CD4+GzB-
TcRβ+CD4+GzB+
16.35
4.98
70.02
9.28
51.70
14.92
29.08
4.25
Lag-3
CD49b
LAG3+CD49b-
LAG3+CD49b+
% CD4+
non-infected total CD4+
infected CD4+GzB+ gated
D
non-infected ctr
infected GzB-
infected GzB+
counts
Tim-3
%Tim3+CD4+
ctr
Infect GzB-
Infect GzB+
E
non-infected ctr
infected GzB-
infected GzB+
counts
CD27
%CD27+CD4+
ctr
Infect GzB-
Infect GzB+
F
NKG2A/C/E
gated CD4+GzB+
gated CD4+GzB-
20.61 %
11.53 %
5.92 %
GzB
GzB+
GzB-
NKG2 A/C/E
CD4
% NKG2A/C/E+ cells
CD4+ non-infected
CD4+ GzB- infected
CD4+GzB+ infected
CD4-
CD4+GzB-
CD4+GzB+
G
NKG2D
gated CD4+GzB+
gated CD4+GzB-
30.51 %
4.12 %
2.09 %
GzB
GzB+
GzB-
NKGD2
CD4
% NKG2D+ cells
CD4+ non-infected
CD4+ GzB- infected
CD4+GzB+ infected
CD4-
CD4+GzB-
CD4+GzB+
H
CRTAM
gated CD4+GzB+
gated CD4+GzB-
21.24 %
10.03 %
3.86 %
GzB
GzB+
GzB-
CRTAM
CD4
% CRTAM+ cells
CD4+ non-infected
CD4+ GzB- infected
CD4+GzB+ infected
CD4-
CD4+GzB-
CD4+GzB+

Figure 4

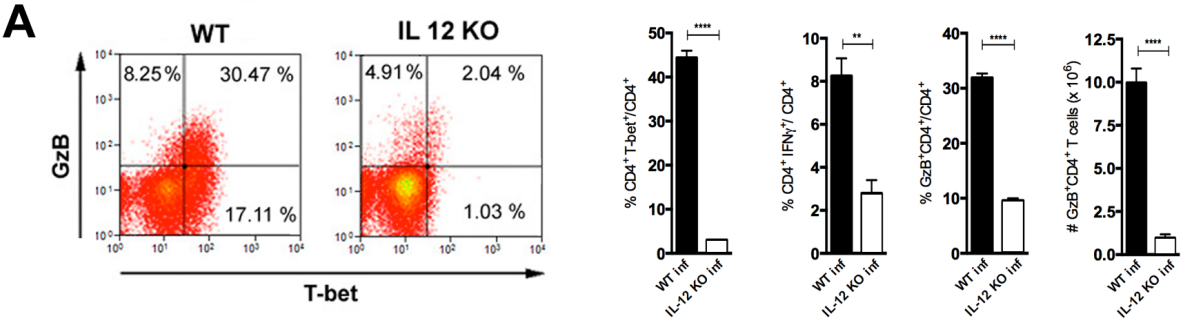
A
WT
IL 12 KO
8.25 %
30.47 %
17.11 %
4.91 %
2.04 %
1.03 %
GzB
T-bet
% CD4+ T-bet+/CD4+
% CD4+ IFNγ+/ CD4+
% GzB+CD4+/CD4+
# GzB+CD4+ T cells (x 10^6)
WT inf
IL-12 KO inf

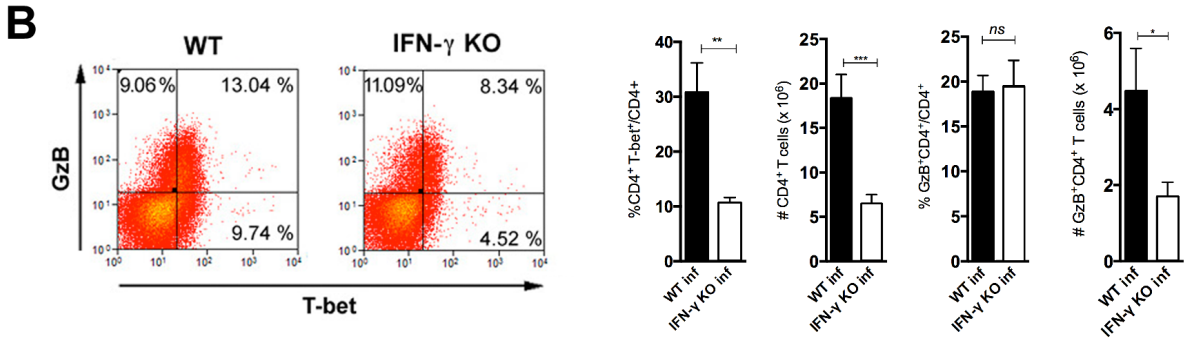
B
WT
IFN-γ KO
9.06 %
13.04 %
9.74 %
11.09%
8.34 %
4.52 %
GzB
T-bet
%CD4+ T-bet+/CD4+
CD4+ T cells (x 10^6)
% GzB+CD4+/CD4+
# GzB+CD4+ T cells (x 10^6)
ns
WT inf
IFN-γ KO inf

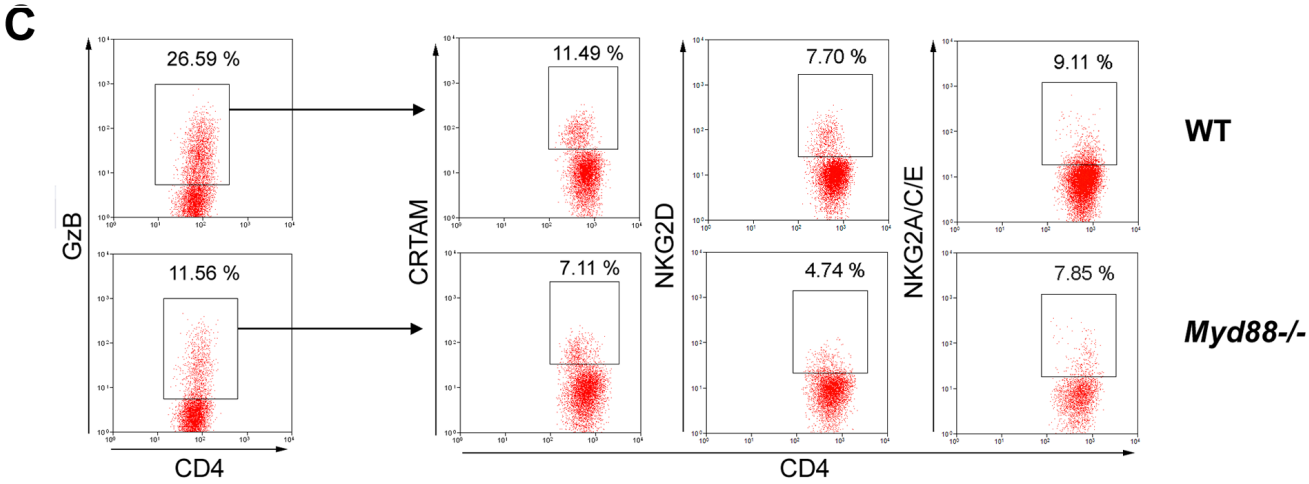
C
26.59 %
11.56 %
11.49 %
7.11 %
7.70 %
4.74 %
9.11 %
7.85 %
GzB
CRTAM
NKG2D
NKG2A/C/E
CD4
WT
Myd88-/-

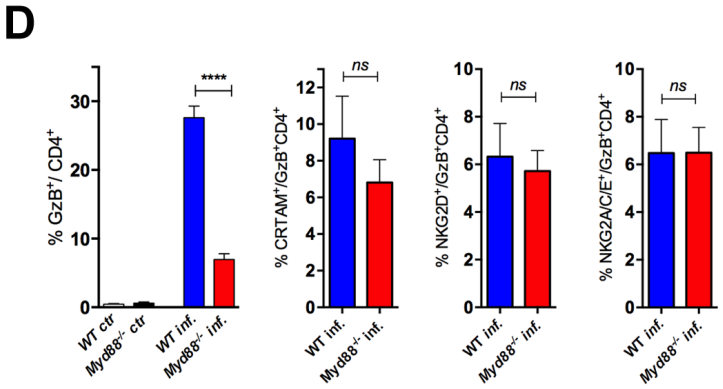
D
% GzB+/ CD4+
% CRTAM+/GzB+CD4+
% NKG2D+/GzB+CD4+
% NKG2A/C/E+/GzB+CD4+
ns
WT ctr
Myd88-/- ctr
WT inf.
Myd88-/- inf.

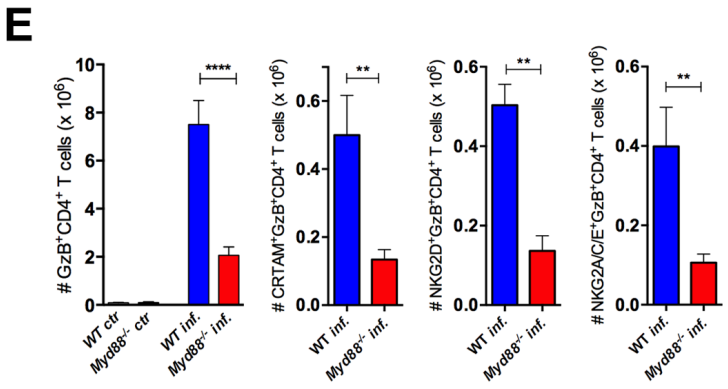
E
GzB+CD4+ T cells (x 10^6)
CRTAM+GzB+CD4+ T cells (x 10^6)
NKG2D+GzB+CD4+ T cells (x 10^6)
NKG2A/C/E+GzB+CD4+ T cells (x 10^6)
WT ctr
Myd88-/- ctr
WT inf.
Myd88-/- inf.

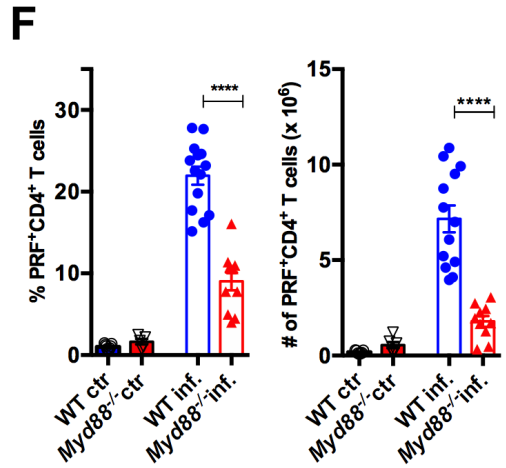
F
% PRF+CD4+ T cells
# of PRF+CD4+ T cells (x 10^6)
WT ctr
Myd88-/- ctr
WT inf.
Myd88-/- inf.

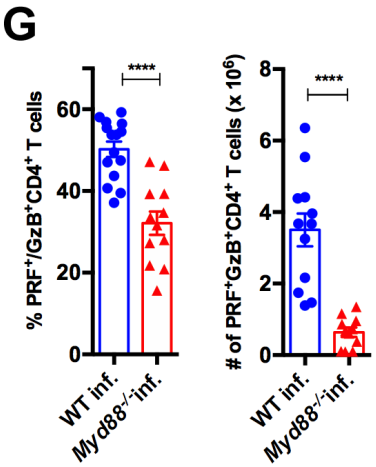
G
% PRF+/GzB+CD4+ T cells
# of PRF+GzB+CD4+ T cells (x 10^6)
WT inf.
Myd88-/- inf.

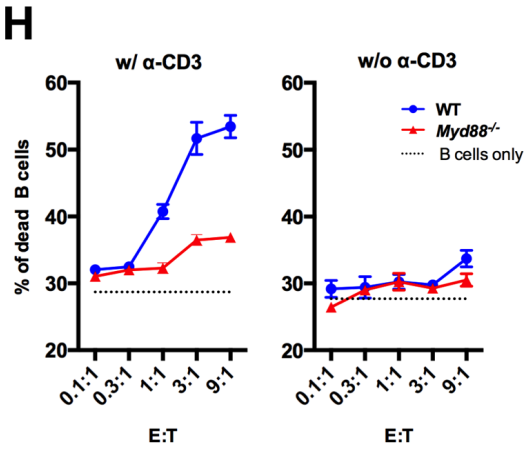
H
w/ α-CD3
w/o α-CD3
% of dead B cells
WT
Myd88-/-
B cells only
0.1:1
0.3:1
1:1
3:1
9:1
E:T

Figure 5

A

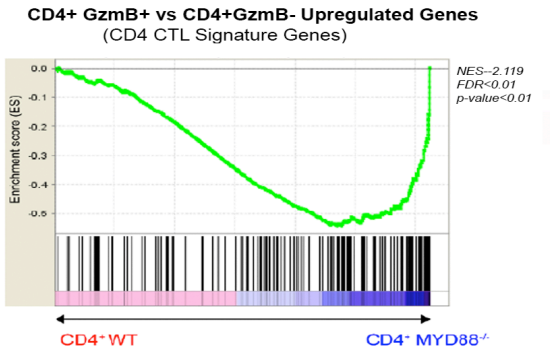

B

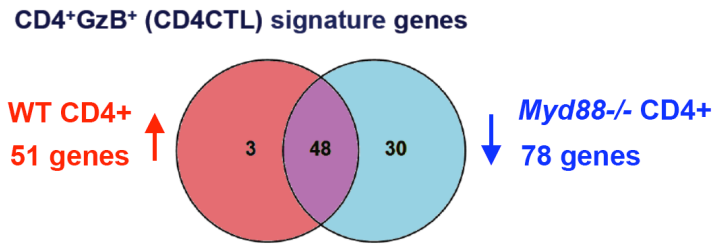

C

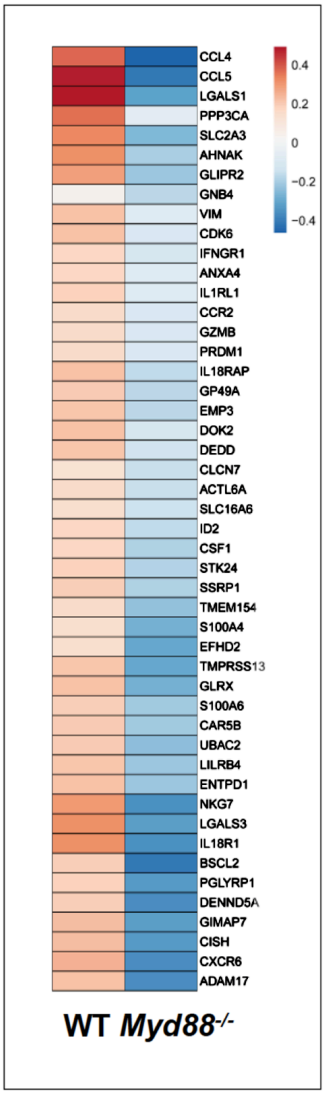

D

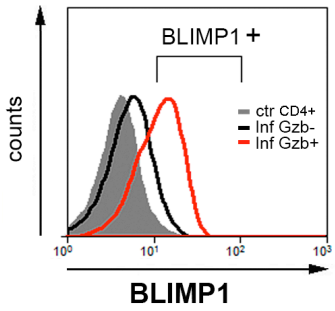

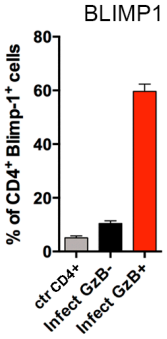

E

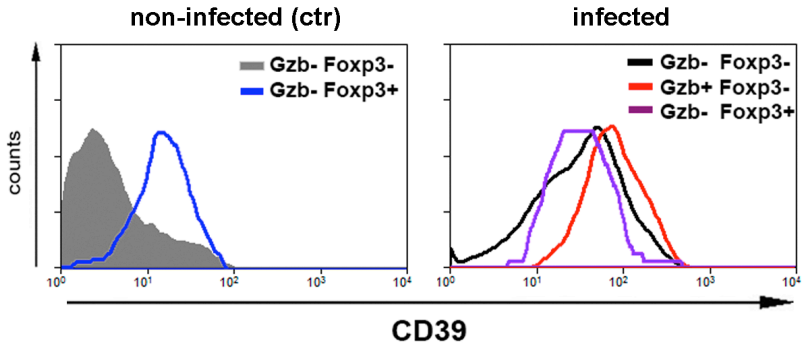

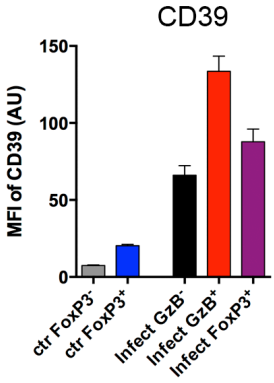

F

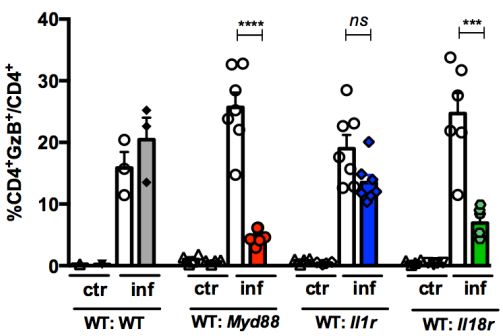

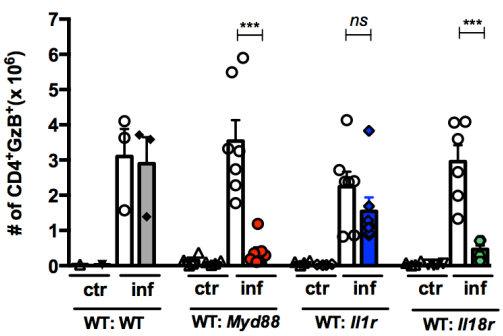

Figure 6

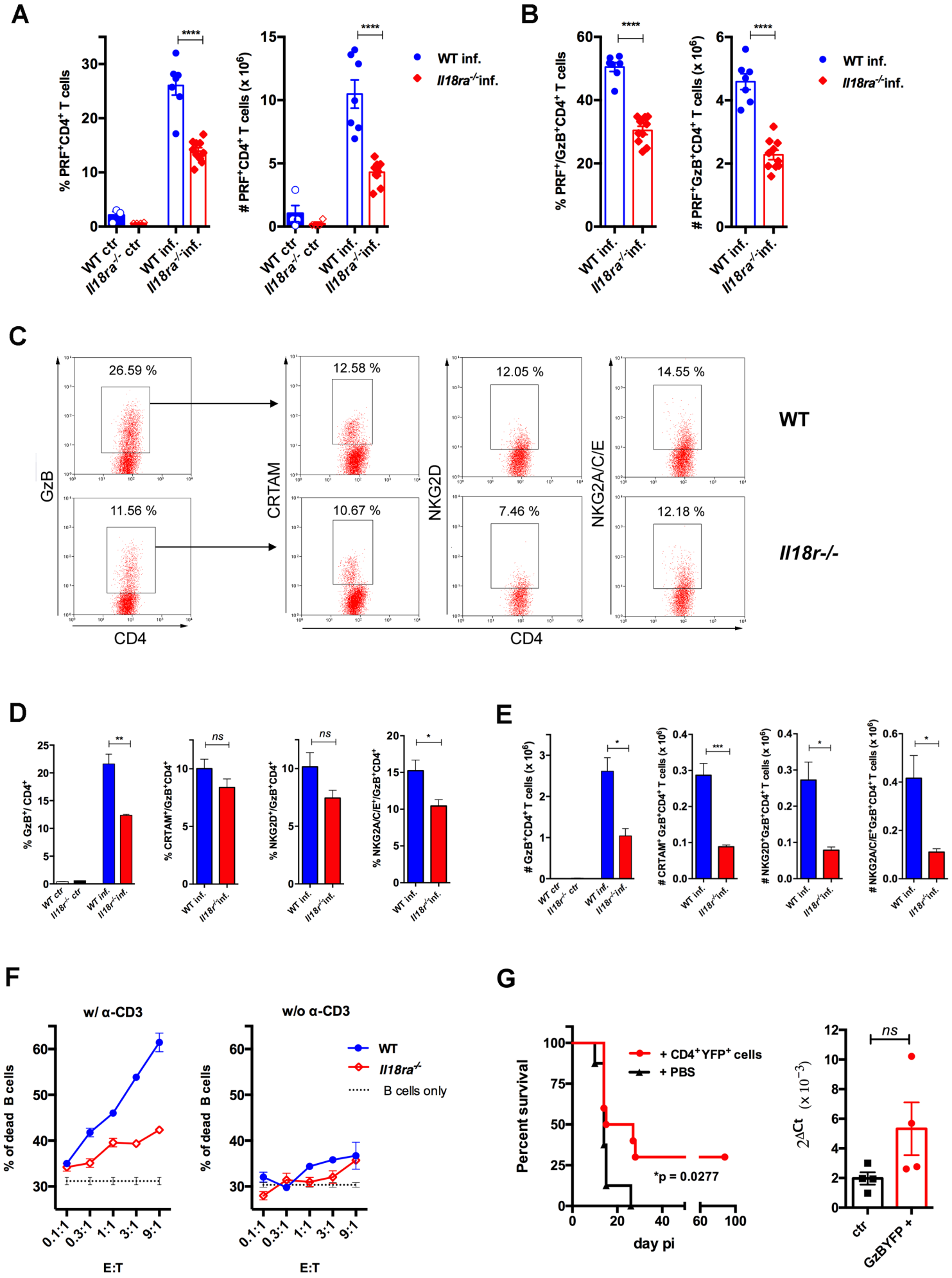
A
% PRF+CD4+ T cells
# PRF+CD4+ T cells (x 10^6)
****
WT ctr
Il18ra-/- ctr
WT inf.
Il18ra-/-inf.
WT inf.
Il18ra-/-inf.
B
% PRF+/GzB+CD4+ T cells
# PRF+GzB+CD4+ T cells (x 10^6)
C
26.59 %
11.56 %
12.58 %
10.67 %
12.05 %
7.46 %
14.55 %
12.18 %
GzB
CRTAM
NKG2D
NKG2A/C/E
CD4
WT
Il18r-/-
D
% GzB+/ CD4+
% CRTAM+/GzB+CD4+
% NKG2D+/GzB+CD4+
% NKG2A/C/E+/GzB+CD4+
ns
E
GzB+CD4+ T cells (x 10^6)
CRTAM+ GzB+CD4+ T cells (x 10^6)
NKG2D+GzB+CD4+ T cells (x 10^6)
NKG2A/C/E+GzB+CD4+ T cells (x 10^6)
F
w/ α-CD3
w/o α-CD3
% of dead B cells
E:T
0.1:1
0.3:1
1:1
3:1
9:1
WT
Il18ra-/-
B cells only
G
Percent survival
day pi
+ CD4+YFP+ cells
+ PBS
*p = 0.0277
2ΔCt (x 10^-3)
ctr
GzBYFP +

Figure 7

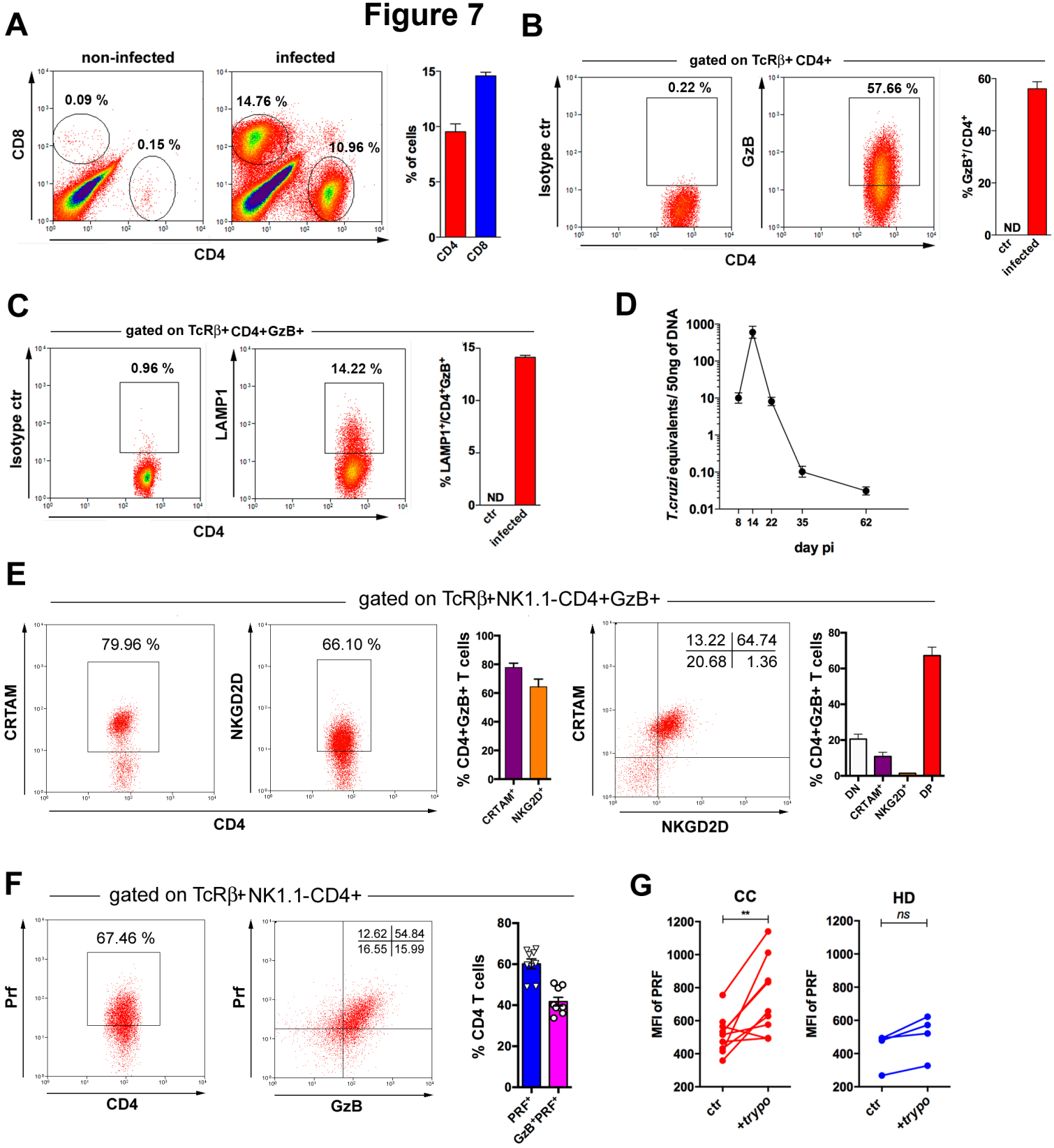
A
non-infected
infected
CD8
CD4
0.09 %
0.15 %
14.76 %
10.96 %
% of cells
CD4
CD8
B
gated on TcRβ+ CD4+
Isotype ctr
GzB
0.22 %
57.66 %
% GzB+/CD4+
ND
ctr
infected
C
gated on TcRβ+CD4+GzB+
Isotype ctr
LAMP1
0.96 %
14.22 %
% LAMP1+/CD4+GzB+
ND
ctr
infected
D
T.cruzi equivalents/ 50ng of DNA
day pi
E
gated on TcRβ+NK1.1-CD4+GzB+
CRTAM
NKGD2D
79.96 %
66.10 %
% CD4+GzB+ T cells
CRTAM+
NKG2D+
13.22
64.74
20.68
1.36
DN
CRTAM+
NKG2D+
DP
F
gated on TcRβ+NK1.1-CD4+
Prf
CD4
GzB
67.46 %
12.62
54.84
16.55
15.99
% CD4 T cells
PRF+
GzB+PRF+
G
CC
HD
ns
MFI of PRF
ctr
+trypo
H
CC
HD
ns
% PRF+CD4+ T cells
ctr
+trypo
I
% PRF+CD4+ T cells
HD
CC
J
LVEF%
p= 0.04
r= -0.62
% PRF+ CD4+ T cells
Left atrium (mm)
p= 0.05
r= 0.80
% PRF+ CD4+ T cells